

Short-term consumption of highly processed diets varying in macronutrient content impair the sense of smell and brain metabolism in mice



Melanie Makhoul^{1,9}, Débora G. Souza^{2,3,9}, Smija Kurian^{1,9}, Bruna Bellaver^{2,9}, Hillary Ellis⁴, Akihito Kuboki⁴, Asma Al-Naama¹, Reem Hasnah^{1,8}, Gianina Teribele Venturin³, Jaderson Costa da Costa³, Neethu Venugopal¹, Diogo Manoel¹, Julie Mennella⁴, Johannes Reisert⁴, Michael G. Tordoff^{3,10}, Eduardo R. Zimmer^{2,3,5,6,7,*,10}, Luis R. Saraiva^{1,4,8,*,10}

ABSTRACT

Objective: Food processing greatly contributed to increased food safety, diversity, and accessibility. However, the prevalence of highly palatable and highly processed food in our modern diet has exacerbated obesity rates and contributed to a global health crisis. While accumulating evidence suggests that chronic consumption of such foods is detrimental to sensory and neural physiology, it is unclear whether its short-term intake has adverse effects. Here, we assessed how short-term consumption (<2 months) of three diets varying in composition and macronutrient content influence olfaction and brain metabolism in mice.

Methods: The diets tested included a grain-based standard chow diet (CHOW; 54% carbohydrate, 32% protein, 14% fat; #8604 Teklad Rodent diet, Envigo Inc.), a highly processed control diet (hpCTR; 70% carbohydrate, 20% protein, 10% fat; #D12450B, Research Diets Inc.), and a highly processed high-fat diet (hpHFD; 20% carbohydrate, 20% protein, 60% fat; #D12492, Research Diets Inc.). We performed behavioral and metabolic phenotyping, electro-olfactogram (EOG) recordings, brain glucose metabolism imaging, and mitochondrial respirometry in different brain regions. We also performed RNA-sequencing (RNA-seq) in the nose and across several brain regions, and conducted differential expression analysis, gene ontology, and network analysis.

Results: We show that short-term consumption of the two highly processed diets, but not the grain-based diet, regardless of macronutrient content, adversely affects odor-guided behaviors, physiological responses to odorants, transcriptional profiles in the olfactory mucosa and brain regions, and brain glucose metabolism and mitochondrial respiration.

Conclusions: Even short periods of highly processed food consumption are sufficient to cause early olfactory and brain abnormalities, which has the potential to alter food choices and influence the risk of developing metabolic disease.

© 2024 The Authors. Published by Elsevier GmbH. This is an open access article under the CC BY-NC-ND license (<http://creativecommons.org/licenses/by-nc-nd/4.0/>).

Keywords Highly processed food; Diet; Olfaction; Metabolism; Obesity

1. INTRODUCTION

The evolutionary history of modern humans is riddled with seismic shifts in their patterns of food, production, consumption, and physical activity [1,2]. The rapid evolution of food processing, driven by industrialization and globalization of food systems in recent decades,

has led to a wide range of processed foods, which greatly enhanced both food security (i.e., enough food for everyone) and nutrition security (i.e., adding important nutrients to processed foods) [3,4]. Presently, a substantial proportion of individuals in Western societies lead sedentary lifestyles within a fast-paced environment, constantly exposed to a multitude of sensory cues that promote the excessive consumption of


¹Sidra Medicine, PO Box 26999, Doha, Qatar ²Graduate Program in Biological Sciences: Biochemistry, Universidade Federal do Rio Grande do Sul (UFRGS), Porto Alegre, Brazil ³Brain Institute of Rio Grande do Sul, Pontifical Catholic University of Rio Grande do Sul, Porto Alegre, Brazil ⁴Monell Chemical Senses Center, 3500 Market Street, Philadelphia, PA 19104, USA ⁵Department of Pharmacology, UFRGS, Porto Alegre, Brazil ⁶Graduate Program in Biological Sciences: Pharmacology and Therapeutics, UFRGS, Porto Alegre, Brazil ⁷McGill Centre for Studies in Aging, Montreal, Canada ⁸College of Health and Life Sciences, Hamad Bin Khalifa University, Doha, Qatar

⁹ Equal contribution.

¹⁰ These authors jointly supervised this work.

*Corresponding author. Sidra Medicine, PO Box 26999, Doha, Qatar. E-mails: saraivalmr@gmail.com (L.R. Saraiva).

**Corresponding author. Graduate Program in Biological Sciences: Biochemistry, Universidade Federal do Rio Grande do Sul (UFRGS), Porto Alegre, Brazil. E-mails: eduardo.zimmer@ufrgs.br (E.R. Zimmer).

 (E.R. Zimmer),  (L.R. Saraiva)

Received September 12, 2023 • Revision received October 29, 2023 • Accepted November 10, 2023 • Available online 17 November 2023

<https://doi.org/10.1016/j.molmet.2023.101837>

Abbreviations

CHOW	Grain-based standard chow diet
hpCTR	highly processed control diet
hpHFD	highly processed high-fat diet
WOM	whole olfactory mucosa
OB	olfactory bulb
BRN	brain
CBL	cerebellum
BST	brainstem
HYP	hypothalamus
EOG	electro-olfactogram
CTX	cortex
RNA-seq	RNA-Sequencing
PCA	principal component analysis
HCA	hierarchical clustering analysis
FDR	false discovery rate
DEGs	differentially expressed genes
FC	fold change
log ₂ FC	log ₂ fold change
GO	Gene Ontology
OIT	olfactory investigation time

RAS	risk assessment
VEL	velocity
+MNT	(+)-menthone
EBT	ethyl butyrate
HXT	hexanethiol
HXO	hexanol
IND	indole
IAA	isoamylamine
LIN	linalool
TMA	trimethylamine
VAN	vanillin
PAC	pentyl acetate
DMSO	dimethyl sulfoxide
FDG-PET	¹⁸ F-Fluorodeoxyglucose micro positron-emission tomography
MLEM-3D	maximum likelihood estimation method
PFUSEIT	PMOD v3.8 and the Fuse It Tool
SUVr	standardized uptake value ratio
VOI	volume of interest
RCR	respiratory acceptor control ratio
UCR	uncoupling control ratio
BKY	Benjamini, Krieger and Yekutieli
SEM	standard error of the mean

energy-dense processed foods [5–7]. Prolonged over-consumption of such foods dysregulates the appetite system, leading to weight gain and contributing to a spectrum of noncommunicable diseases, including metabolic disorders, cancer, autoimmune diseases, mental and brain health issues [2,8–11].

Sensory inputs, such as food odors, interact with internal homeostatic and hedonic signals in the brain to regulate food retrieval and ingestive behaviors [6,12–15]. In appetite regulation, olfaction is perhaps the most evocative of all five senses. Indeed, several lines of evidence support the essential role of smell in food detection and then selection, which determines dietary quality, caloric intake, and metabolic health [16–18]. Additionally, olfactory dysfunction (e.g., hyposmia) further stimulates the ingestion of nutrient-poor and energy-dense diets, leading to an unhealthy vicious cycle [19,20]. In turn, the long-term consumption of energy-dense diets (e.g., high-fat or high-fructose diets) can negatively impact olfactory physiology, odor-guided behaviors, and lead to altered brain function in regions involved in olfactory processing [6,12,13,21–27].

Considering the major shifts in eating culture, the prevalence of cheap and readily-available highly processed foods, and the resulting obesity epidemic over the last five decades, it is crucial to map and better understand the effects of not just long-term but also short-term consumption of different diets on health and disease. In laboratory rodents, these questions can be studied by comparing the effects of grain-based standard chow diets (CHOW) with purified-ingredient-based diets, the latter being equivalent to human highly processed foods [28–30]. Interestingly, a recent study showed that mice fed a highly processed macronutrient-balanced control diet (hpCTR) have a lower ability to defend against influenza when compared to animals fed a standard mouse chow diet with a similar macronutrient composition [29]. Moreover, recent studies of mice have shown that consuming a highly processed high-fat diet (hpHFD) for only a few days can lead to metabolic changes (e.g., ketogenesis, hepatic steatosis, insulin resistance), and alter the transcriptional profile of the intestine [31–35].

Despite these recent advances in the field, how the sense of smell and brain function are affected by the short-term consumption of diets

differing in composition and macronutrient content remains largely unknown. To address this question, we used mice to investigate the effects of the short-term consumption (<8 weeks) [36,37] of one grain-based (CHOW), and two highly processed diets (hpCTR and hpHFD) on odor-guided behaviors, olfactory physiology, the transcriptional profiles in the olfactory mucosa and various brain regions, as well as brain glucose metabolism and mitochondrial respiration.

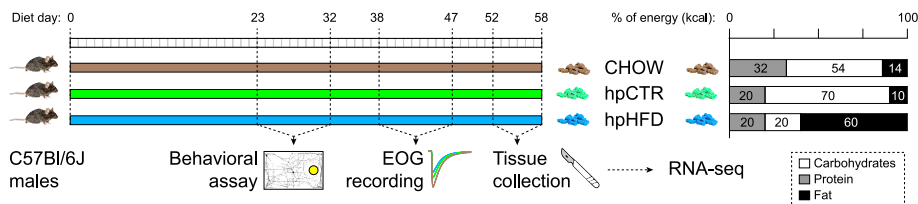
2. MATERIAL AND METHODS

2.1. Animals and dietary interventions

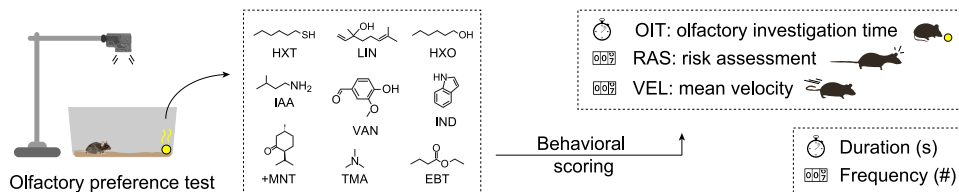
The animals used for this study were male C57Bl/6J mice (The Jackson Laboratory, Stock # 00664) maintained in group-housed conditions on a 12:12 h light:dark schedule (lights on at 07.00 h). Animals were randomized to be fed one of three diets differing in macronutrient content and ingredient composition: a grain-based standard chow diet (CHOW; 54 % carbohydrate, 32 % protein, 14 % fat; #8604 Teklad Rodent diet, Envigo Inc.), a highly processed macronutrient-balanced control diet based on purified ingredients (hpCTR; 70 % carbohydrate, 20 % protein, 10 % fat; #D12450B, Research Diets Inc.), and a highly processed high-fat diet based on purified ingredients (hpHFD; 20 % carbohydrate, 20 % protein, 60 % fat; #D12492, Research Diets Inc.) (see Figure 1A, Additional file 2: Table S1). An analysis of the ingredient composition for the three diets according to the NOVA food classification system [28] revealed that the CHOW diet is composed of 40 % natural or minimally processed ingredients (NOVA Group 1), 40 % processed (NOVA Group 3), and 20 % ultra processed (NOVA Group 4) foods; but the hpCTR and hpHFD are composed exclusively of processed (37.5–44.4 %) and ultra processed (55.6–62.5 %) foods (see Figure S1A, Additional file 2: Table S1).

Mice had *ad libitum* access to food and water throughout the duration of the study. Upon arrival at the Monell Chemical Senses Center animal facility, male C57Bl/6J mice (5 weeks old) were habituated for 5 days, and then randomly assigned to one of the three dietary experimental groups: CHOW (n = 85), hpCTR (n = 72), and hpHFD (n = 79). The dietary intervention lasted 52–58 days – we did so to ensure to

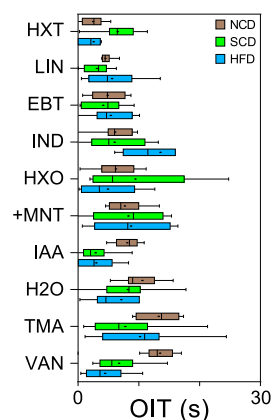
A Experimental strategy and diet composition



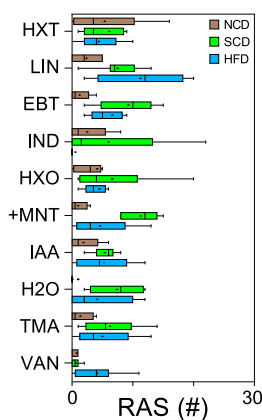
B Behavioral assay



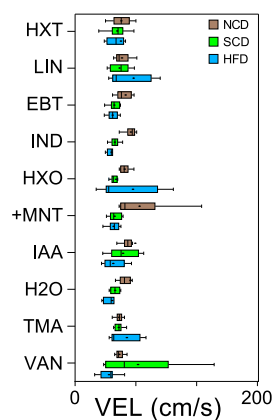
C OIT



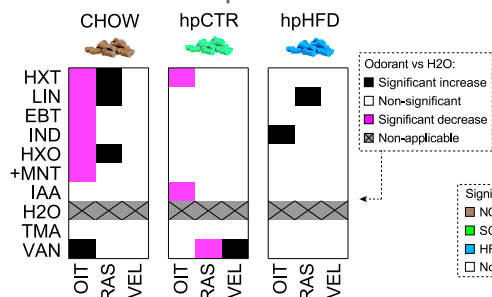
D RAS



E VEL



F Intra-diet comparison



G Inter-diet comparison

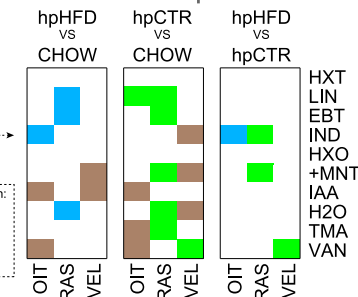


Figure 1: Effects of short-term consumption of diets differing in composition and macronutrient content on odor-guided behaviors. (A) Schematic view of the experimental design for the first part of our study, comprising three different diets: a grain-based “normal” chow diet (CHOW, brown bar), a highly processed control diet (hpCTR, green bar), or a highly processed high-fat diet (hpHFD, blue bar). The macronutrient composition (%) for each diet is depicted on the right (carbohydrates in white, protein in grey, and fat in black). (B) Behavioral assays: animals were exposed to nine odorants, and videos were recorded and scored for three distinct behavioral parameters: olfactory investigation time (OIT), risk assessment (RAS), and velocity (VEL). Odorants used: (+)-menthone (+MNT), ethyl butyrate (EBT), hexanethiol (HXT), hexanol (HXO), indole (IND), isoamylamine (IAA), linalool (LIN), trimethylamine (TMA), vanillin (VAN). (C–E) Boxplots summarizing the behavioral parameter scores for the nine tested odorants. OIT scores are shown in seconds (C), RAS scores in frequencies (D), and VEL scores in distance per second (E). (F) A graphical display in the form of a heatmap summarizing the statistical significance results of intra-diet comparisons. Behaviors showing significant (one-way ANOVA, BKY multiple comparisons correction, $n = 7–12$ per odorant) increases, decreases and non-significant responses compared to H₂O (no odor control) are indicated in black, magenta, and white squares, respectively. Non-applicable comparisons are in grey. (G) A graphical display in the form of a heatmap summarizing the statistical significance of inter-diet comparisons for each odorant-behavioral parameter dyad. Behaviors with significantly higher values (one-way ANOVA, BKY multiple comparisons correction, $n = 7–12$ per odorant) in CHOW, hpCTR or hpHFD diets are indicated in brown, green or blue, respectively. Non-significant responses are indicated in white.

ensure that all animals were eating the assigned randomized diet at the time of dissection (see Figure 1). Upon arrival at the UFRGS animal facility, C57BL/6J male mice (10–12 weeks old) were randomly assigned to one of the three dietary experimental groups: CHOW (n = 9), hpCTR (n = 10), and hpHFD (n = 9).

2.2. Odorants used in this study

The odorants used in this study were purchased from Sigma-Aldrich at the highest purity available. Their names are shown below, followed by their abbreviations in parentheses: (+)-menthone (+MNT), ethyl butyrate (EBT), hexanethiol (HXT), hexanol (HXO), indole (IND), isoamylamine (IAA), linalool (LIN), pentyl acetate (PAC), trimethylamine (TMA), vanillin (VAN). For the behavioral assays, odorants were either diluted in water to a concentration of 85 mM, or first dissolved in dimethyl sulfoxide (DMSO) to make a 1 M stock solution and then diluted in water to a concentration of 85 mM, immediately before the assays. For the electroolfactogram recordings, odorants were first dissolved in DMSO to make a 5 M stock solution, then diluted in water to obtain odorant solutions at 10^{-2} M in 5 mL final volumes in sealed 50 mL glass bottles. As a control (0 M odorant), a solution of DMSO equivalent to the concentration in the 10^{-1} M odorant solution was used.

2.3. Olfactory preference test and behavioral scoring

The olfactory preference tests were performed at Monell Chemical Senses Center, 22–32 days after the start of the dietary treatment on 9–10 week-old mice, as previously described [38] and with minor modifications (see below). Each mouse was assayed only once to avoid possible bias due to learning, and data for each odorant consisted of 7–12 mice. On the day of testing, mice were brought to the experimental room 120–180 min prior to the onset of the dark cycle (at 19:00) and habituated for 5–10 min. Mice were then separated into new cages (one mouse per cage) without food or water and habituated again for 15–30 min. Exposure to odorants was done by gently introducing a stainless-steel mesh tea ball containing a cotton ball impregnated with 50 μ L of double-distilled water (H₂O) or odorant (85 mM in H₂O, equivalent to 4.25 μ mol), into one end of the cage. Videos were recorded from the top, for slightly over 3 min, using a GoPro HERO6 Black camera (Waterproof Digital Action Camera for Travel with Touch Screen 4K HD Video). All behavioral assays were conducted during the last 2 h of the light cycle, between 17:00 and 19:00.

Prior to scoring, all videos were cropped with a custom-made tool developed in our lab — the “Video Crop” tool (<https://github.com/NeethuVenugopal/vidocrop>) — to eliminate areas around the mouse cage that will interfere with the downstream automated video tracking done using Ethovision XT software (version 11, Noldus Information Technology). Briefly, the “Video Crop” tool is a script encoding a video cropping tool that provides a graphical user interface (GUI) for users to select a specific region of interest (ROI) in a video. By interactively clicking and dragging the mouse, users can define the ROI on the video frames. Once the selection is confirmed, the script crops the frames within the ROI and saves the cropped video as an output file. This tool enables users to extract specific portions of a video, focusing only on the desired content.

The behavioral parameters of each mouse/video were scored by a non-experimenter blinded to the odor used in the assay. Three behavioral parameters were scored during a 3-minute period, starting from introducing the odorant-containing metal tea ball:

- Olfactory investigation time (OIT) represents the cumulative duration of olfactory investigation during the assay duration. This parameter is a surrogate measure for valence [39], and scored using the Ethovision XT software (version 11, Noldus Information Technology) with the video tracking done using the nose-point of the mice. An automated detection setting based on greyscale analysis was used to detect mice in this analysis, and olfactory investigation was considered only if the nose-point of the mice was touching the odorant-containing tea ball.
- Risk assessment (RAS) represents the number of episodes the mouse displays the flat-back/stretch-attend response, followed by a sniff in the direction of the stimulus, during the assay duration. This parameter is a surrogate measure for stress [39], and was scored manually.
- Velocity (VEL) represents the mean velocity at which the mouse walked/ran during the assay duration. This parameter is a surrogate measure for activity [39], and scored using the Ethovision XT software (version 11, Noldus Information Technology) with the video tracking done using the center-point of the mouse. An automated detection setting based on greyscale analysis was used to detect mice in this analysis (refer to Ethovision guide).

2.4. Electro-olfactogram recordings

The electro-olfactogram (EOG) recordings were performed at Monell Chemical Senses Center, 38–47 days after the start of the dietary treatment on 10–11 week-old mice, as previously described [40] and with minor modifications (see below). Data for each dietary group was based on 7–8 mice. The mice were euthanized with CO₂ and decapitated, and their heads were sagittally bisected at the center of the nasal septum. The septum was removed to expose the olfactory turbinates in the nasal cavity. The bisected heads were quickly transferred to a recording setup, where a stream of humidified air flowed (3 L/min) over the tissue.

In these experiments, we used the odorants PAC, VAN, IND, HXT, IAA, +MNT, LIN, EBT, and TMA. The headspace from each odorant solution was injected with a Picospritzer (Parker Hannifin, Cleveland, OH, USA) into the air stream flowing over the OE to stimulate OSNs. EOG recordings were performed in the order of PAC, VAN, IND, HXT, IAA, PAC, +MNT, H₂O, LIN, EBT, TMA, DMSO control solution, and PAC again as a control for recording stability over time. To record the EOGs, two electrodes were placed on the surfaces of turbinate II and IIB respectively using either the left or right half of the head at similar positions in all mice [41]. The signals were recorded with two DP-301 amplifiers (Warner Instruments, Hamden, CT, USA), and the 1 kHz low-pass-filtered signal was digitized at 2 kHz with a Micro1401 mkII digitizer and Signal version 5.01 software (Cambridge Electronic Design, Milton, Cambridge, England). Recordings were analyzed by averaging across the four channels recorded from both sides of the nasal cavity. If there was more than a 25 % reduction in the response amplitude between the first PAC and the last PAC recording from a given electrode, the data were excluded. On occasions, mice had nasal cavities with strongly deviating septa, which typically gave small responses, and these data were also excluded.

2.5. Tissue dissection, RNA extraction, and RNA-sequencing

Tissue dissections were performed at Monell Chemical Senses Center, 52–58 days after the start of the dietary treatment on 12–13 week-old mice. All animals were sacrificed by cervical dislocation between

14:00 and 16:00). From each animal, the following tissue samples were collected and processed for mRNA-seq: whole olfactory mucosa (WOM), dissected as described in [42], olfactory bulb (OB), brain (BRN, which includes the telencephalon and diencephalon), cerebellum (CBL), brainstem (BST, which consists of the mesencephalon, pons, and myelencephalon). The organs were immediately frozen and kept at -80°C until further processing.

WOM, OB, BRN, CBL, and BST samples were homogenized using a tissue homogenizer (OMNI International) in Qiazol (Qiagen). Total RNA for the WOM, OB, BRN, CBL, and BST samples was extracted using the Lipid RNeasy Lipid Tissue Mini Kit (Qiagen), according to the manufacturer's protocol. mRNA was prepared for sequencing using the TruSeq stranded mRNA sample preparation kit (Illumina), with a selected insert size of 120–210 bp. Stranded libraries were sequenced on an Illumina HiSeq 4000, generating paired-end 150 bp sequencing reads, with an average depth of 45 ± 1.4 (SEM) million reads.

2.6. Short read alignment to the reference genome and transcriptome

The quality of the reads was assessed using FastQC (KBase). Sample Fastq files were aligned to the mouse reference genome GRCm38.p6 (GCA_000001635.8) using TopHat2 (version 2.1.1) [43] with 2 mismatches allowed. Reads were retained only if uniquely mapped to the genome. We used HTSeq-count (0.9.1, -t exon and -m union) to obtain the number of reads that were mapped to each gene in Gencode M24. Bigwig files were generated from bam files for visualization using bam2wig.py function RSeQC v3.0.1 [44].

2.7. Differential expression analysis and functional annotation

Sample transcriptome data quality was assessed by evaluating homogeneity and similarity between samples. We used variance stabilizing transformation (vst) and regularized log transformation (rlog) functions (DESeq2 package, v1.26.0) [45] to transform the raw count data, (dist) function to calculate sample-to-sample distances. We plotted heatmaps of distance matrix along with PCA of 1000 HVG and the union of the top 1000 most expressed genes to identify putative outlier samples. These samples if present were excluded from the following differential expression analyses. We also used DESeq2 (v1.26.0) to normalize the raw count matrix according to sequencing depth and RNA composition (median of ratios method), then to perform differential expression analysis. Differential expression was tested using the DESeq function from the DESeq2 library, which employs the Wald test to determine if the \log_2 fold change in gene expression across two groups of samples is higher than expected by chance. Finally, DESeq does p-value correction (adjusted p-value) for multiple testing. Genes with a $\text{padj} < 0.05$ and $|\log_2\text{FC}| > 1$ were considered as differentially expressed. Gene over-representation analysis was performed using ClusterProfiler package (v4.0.0) (PMID: 34557778). We used Gene Ontology enrichment (enrichGO) and Simplify functions, with $\text{ont} = \text{"BP", "MF" or "CC"}$ and $\text{pAdjustMethod} = \text{"BH"}$ parameters to assess which Biological Processes, Molecular Functions, or Cellular Components were affected in our lists of differentially expressed genes.

2.8. ^{18}F -Fluorodeoxyglucose micro positron-emission tomography (FDG-PET) scanning

These experiments were performed at UFRGS, 25 days after the start of the dietary treatment on 14–16-week-old mice, as previously described [46] and with minor modifications (see below). After overnight fasting (12 h, from 08:00 PM to 08:00 AM), the mice received an intravenous

injection (0.4 mL) of FDG-PET (mean \pm s.d.: 0.26 ± 0.006 mCi) in the tail vein. Then, each mouse was returned to its home cage for a 40-minute period of conscious (awake) *in-vivo* FDG uptake, followed by a 10-minute static acquisition under anesthesia (2 % isoflurane at 0.5 L/min oxygen flow). FDG-PET measurements were performed on a Triumph™ micro-PET [LabPET-4, TriFoil Imaging, Northridge, CA, USA (for LabPET-4 technical information see [47]). The brain was positioned in the center of the field of view (FOV; 3.75 cm), and the body temperature was maintained at $36.5 \pm 1^{\circ}\text{C}$. All data were reconstructed using the maximum likelihood estimation method (MLEM-3D) algorithm with 20 iterations. Each FDG-PET image was reconstructed with a voxel size of $0.2 \times 0.2 \times 0.2$ mm and spatially normalized into an FDG-PET template using brain normalization in PMOD v3.8 and the Fuse It Tool (PFUSEIT) (PMOD Technologies, Zurich, Switzerland). The following imaging analysis was conducted using the minc-tools software (www.bic.mni.mcgill.ca/ServicesSoftware/MINC). The standardized uptake value ratio (SUVr) was calculated using pons as the reference region. Mean SUVrs of the four analyzed brain regions were extracted using a predefined volume of interest (VOI) template.

2.9. Glucose tolerance test

The glucose tolerance test experiments were performed at UFRGS, 27 days after the start of the dietary treatment when mice were 11-week of age, as previously described [48], and with minor modifications (see below). In brief, after an overnight fast (12 h, from 08:00 PM to 08:00 AM), a 2 g/kg glucose solution was orally administered and tail vein blood glucose was measured with the Accu-Chek Active meter at baseline (time 0), and at fixed intervals thereafter (i.e., 15, 30, 60, and 120 min).

2.10. High-resolution mitochondrial respirometry

These experiments were performed at UFRGS 30 days after the start of the dietary treatment on 13–15-week-old mice, as previously described [49], and with minor modifications (see below). Mice were euthanized by decapitation, had their HYP, OB and cortex (CTX) rapidly dissected and put on ice. Representative slices of all cortical regions, and the complete hypothalamus and olfactory bulbs were weighted, homogenized 10 % (w/v) in respiration buffer (MirO5 - 110 mM sucrose, 60 mM potassium lactobionate, 20 mM taurine, 10 mM monobasic potassium phosphate, 3 mM magnesium chloride, 20 mM HEPES, 1 mM EGTA, and 0.1 % (w/v) BSA at pH 7.1) using a glass potter (10–12 strokes on ice). Samples were transferred to an oxygraph-2k (O2k, Oroboros Instruments, Innsbruck, Austria) in 100–200 μg total protein per chamber at 37°C and initial O_2 concentration of around 200 μM . Substrate, uncoupler, inhibitor titration (SUIT) protocol was carried out in MirO5 (adapted from [50]): respiratory states were induced with pyruvate 5 mM, malate 4 mM, and glutamate 10 mM. Oxidative phosphorylation activity was measured with ADP 500 μM and succinate 10 mM. Oligomycin 0.2 $\mu\text{g}/\text{mL}$ (Omy), an ATP synthase inhibitor, was used to determine leak respiration. Titration of the uncoupler carbonyl cyanide m-chlorophenyl hydrazone (CCCP) 0.5 μM allowed verification of maximal O_2 consumption. Complex I inhibition was obtained with rotenone 0.5 μM (R). Residual consumption was induced with antimycin A 2.5 μM (AA). The remaining oxygen consumption after R and AA was considered non-mitochondrial respiration.

Respirometry was analyzed with the DatLab software (v6.1.0.7. Oroboros Instruments). Respiratory acceptor control ratio (RCR) was defined by the coupling state of mitochondria obtained by the division of the O_2 flux in the presence of substrates and ADP (OXPHOS — state 3) by the O_2 flux after Omy addition (state 4). OXPHOS capacity is the

oxidation coupled to phosphorylation in the presence of saturating O₂, ADP, and substrate concentration. Proton leak is a dissipative component of respiration that is not available for performing biochemical work and is thus related to heat production. Uncoupling control ratio (UCR) is the ratio between the maximum respiratory capacity achieved under uncoupler titration (CCCP) and the O₂ flux during proton leak [51].

2.11. Statistical analysis

Statistical analyses were done using R Statistical Software (version 4.1.0.), GraphPad Prism (version 8.0.0), and Origin software version 8.5 (Origin Lab, Northampton, MA, USA), or PALaeontological Statistics (version 4.06, <http://folk.uio.no/ohammer/past/>). For the principal component analysis (Figure 2C and Additional file 1: Figures S2A and B), the data matrix was standardized, and correlation matrixes used to

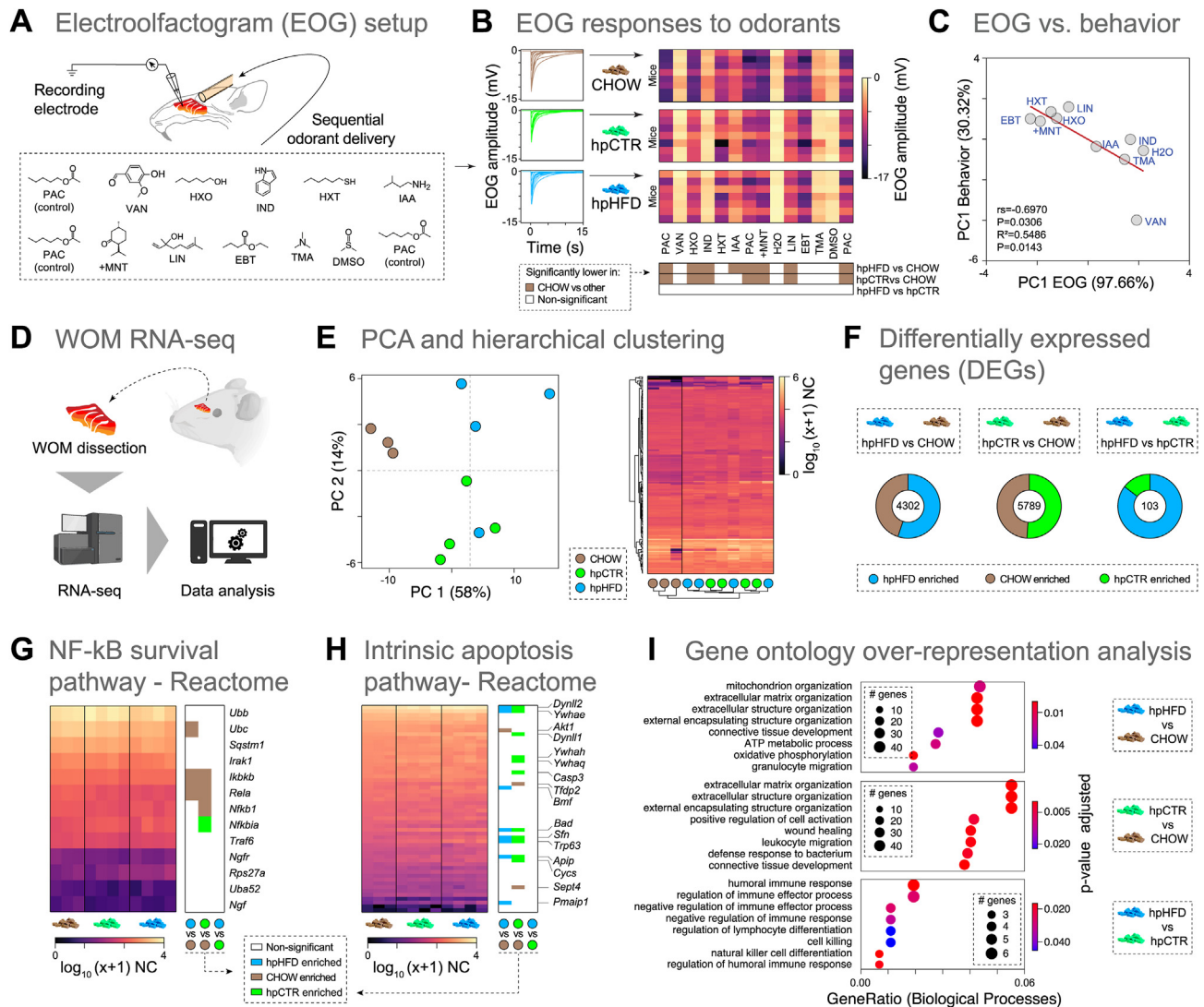


Figure 2: Highly processed diets affect odorant detection and induce transcriptional dysregulations in the mouse nose. (A) Schematic of the air-phased electroolfactogram (EOG) recording experiments performed with 11 odorants on mice exposed to the three test diets (CHOW, hpCTR or hpHFD). (B) Left panel: Odorant-evoked EOG response curves to odorants. Upper right panel: Heatmap showing the odorant evoked EOG amplitude values (mV) per mouse. Lower right panel: Heatmap summarizing the statistical significance of the comparison of peak amplitudes in EOG recordings in response to each odorant between diets. EOG amplitudes showing significantly lower values ($p < 0.05$; two-way ANOVA; BKY multiple comparisons correction, $n = 7-8$ per odorant) in CHOW, hpCTR or hpHFD are indicated in brown, green or blue, respectively. Non-significant responses are indicated in white. (C) Spearman correlation (r_s) and linear regression (R^2) between principal component 1 (PC1) of the EOG responses and PC1 of the odor-guided behaviors. (D) Schematic view of the RNA-seq experimental strategy for the whole olfactory mucosa (WOM) samples ($n = 3-4$ mice per group). (E) PCA and hierarchical clustering of the union of the top 1000 most expressed genes across all WOM samples. Heatmap RNA-seq expression values are represented on a $\log_{10}(x+1)$ scale of normalized counts (NC). Each dot represents an animal. (F) Pie chart displaying the total number and relative proportion of differentially expressed genes (DEGs; $p\text{-adj} < 0.05$) for each pairwise diet comparison in the WOM. Genes enriched in mice fed on CHOW, hpCTR or hpHFD are indicated in brown, green or blue, respectively. (G-H) Heatmap (left panel) showing the normalized gene expression levels of Reactome “NF- κ B is activated and signals survival” pathway (G) or the Reactome “intrinsic apoptosis” pathway genes (H). Right panels: a graphical display in the form of a heatmap summarizing the statistical significance of inter-diet comparisons. DEGs enriched in mice fed on CHOW, hpCTR or hpHFD are indicated in brown, green or blue, respectively. (I) Dot plot representing selected significant terms from Gene Ontology (GO) over-representation analysis done on DEGs ($\log_2(FC) > 1$, $p\text{-adj} < 0.05$) from differential expression analysis between diets. Enriched terms are displayed by gene ratio (number of genes related to a GO term/total number of significant genes). The size of the dot reflects the number of genes enriched within the associated GO term, and its color reflects the p -adjusted value for each term.

compute the eigenvalues and eigenvectors. Results were analyzed by one-way or two-way ANOVA, and P-values were computed with Benjamini, Krieger and Yekutieli (BKY) multiple comparisons correction (P-values <0.05 were considered significant).

3. RESULTS

3.1. Short-term consumption of highly processed diets severely impact odor-guided behaviors

Long-term unhealthy dietary interventions can lead to impairments in memory, and emotional or cognitive behaviors (such as reward-, social- and stress-related behaviors), even independently of obesity [11,23,26,52–55]. The long-term consumption of high-fat, high-fructose, or Western diets can also lead to defects in specific olfactory-related behaviors, such as odor discrimination, odor-related learning, and memory [23,24,27,55,56]. However, whether the short-term consumption of highly processed diets can affect the sense of smell remains unknown.

To address this question, we randomly allocated C57Bl/6J male mice to one of the three ultra-processed diets that differ in ingredient origin and macronutrient composition: a grain-based “normal” chow diet (CHOW), a highly processed control diet (hpCTR), or a highly processed high-fat diet (hpHFD) (see Methods, Figure 1A, Additional file 2: Table S1). Mice fed the hpHFD weighed significantly more than mice fed the CHOW or the hpCTR (Figure S1). After being on their designated diet for three weeks, we performed olfactory preference behavioral tests against an odorless control (water, H₂O) and nine odorants (hexanethiol, HXT; linalool, LIN; hexanol, HXO; isoamylamine, IAA; vanillin, VAN; indole, IND; (+)-menthone, +MNT; trimethylamine, TMA; ethyl butyrate, EBT). These odorants have different chemical structures, functional groups, and have previously been shown to elicit a range of behavioral outputs in mice [38,39]. To avoid habituation, each mouse was used only once and against one odorant (n = 7–12 mice per odorant) and scored on three different behavioral parameters considered surrogates for odor “valence” (OIT, olfactory investigation time), stress (RAS, risk assessment), and exploration (VEL, velocity) (Figure 1B). This dataset totaled 722 data points corresponding to individual-odorant-behavior triads (Figure 1C–E and S1A, Data S1), for which we calculated the average value for each of the 30 odorant-behavior pairs for each tested diet. Surprisingly, the patterns of significant increases and decreases compared to H₂O (p < 0.05; one-way ANOVA; BKY multiple-comparisons correction) across the different behaviors differ across the three different diets, with CHOW displaying the highest number of differences (10), followed by hpCTR (4) and hpHFD (2) (Figure 1F). Only 2 of the 16 significant odorant-induced behavioral changes were shared between at least two diets: the significant decrease of OIT for HXT (in CHOW and hpCTR) and the significant increase of RAS for LIN (in CHOW and hpHFD). Next, we compared the same odorant-behavior pairs between diets (Figure 1G), and found unique behavioral differences amongst pairwise diet comparisons. The highest number of significant behavioral differences (13) was observed in the hpCTR vs. CHOW, followed by 8 in hpHFD vs. CHOW, and 4 in hpHFD vs. hpCTR. In both comparisons vs. CHOW most OIT and VEL differences were significantly higher in CHOW, but all RAS differences were significantly higher in hpCTR and hpHFD. In hpHFD vs. hpCTR, the only OIT difference was significantly higher in hpHFD, and the differences in RAS and VEL were all significantly higher in hpCTR. Moreover, each diet displayed unique patterns of significant changes among the three behaviors tested.

Together, these results indicate that short-term dietary interventions can substantially impact odor-guided behaviors in mice, with highly processed diets strongly impacting their standard olfactory preferences, and mildly increasing their stress-related behavior.

3.2. The short-term consumption of highly processed diets impair odorant detection in the nose

Internal metabolic signals can directly modulate the response of olfactory sensory neurons (OSNs) to odorants [22,57]. Thus, the behavioral deficits observed in animals fed the hpCTR and hpHFD could be due, at least in part, to changes in the peripheral detection of odorants in the neuroepithelium of the mouse olfactory mucosa. To test this hypothesis, we performed air-phased electro-olfactogram (EOG) recordings in response to the nine odorants used in the behavioral assays, two control odorants (pentyl acetate, PAC; dimethyl sulfoxide, DMSO) (Figure 2A). The amplitudes of the odorant responses varied between the three tested diets, with mice on the CHOW displaying significantly larger EOG amplitudes to most odorants compared to hpCTR or hpHFD (p < 0.05; two-way ANOVA, odorants: $F_{(13,266)} = 108.6$, p < 0.0001; Diet: $F_{(2,266)} = 49.2$, p < 0.0001; Interaction: $F_{(26,266)} = 1.51$, p = 0.0564; BKY multiple-comparisons correction; Figure 2B). Interestingly, there were no significant differences in EOG amplitudes between hpCTR and hpHFD, similar to our behavioral results. Together, our data suggest that deficits in peripheral detection of odorants is a result of the processed nature of the diet (or some diet component aligned with this) rather than macronutrient content.

Because we performed behavioral and physiological experiments in the same mice, we next asked whether the dietary-induced changes in odorant detection in the nose are associated with the corresponding odor-guided behaviors. We performed principal component analysis (PCA) on the data matrixes from the EOG responses and the odor-guided behaviors of the nine tested odorants and water (see Methods, Figures S2A and B). Strikingly, we observed a strong correlation (rs = -0.69, p = 0.03) between the PC1 (97.66 % of the variance) of the EOG responses and the PC1 (30.32 % of the variance) of the odor-guided behaviors (Figure 2C). The linear regression analysis ($R^2 = 0.55$, p = 0.01) indicates that the decrease in responsiveness of OSNs to odorants, caused by consuming highly processed diets, accounts for ~55 % in the variation of odor-guided behaviors. Overall, these findings demonstrate that short-term consumption of highly processed food impairs olfactory processing and related behaviors. However, the impairment of olfactory function in the periphery does not fully account for its impact on odor-guided behaviors, suggesting the presence of other contributing mechanisms, likely happening in the brain.

3.3. Highly processed diets induce transcriptional dysregulations associated with apoptosis and inflammatory responses in the mouse nose

To better understand the mechanisms underlying the physiological dysregulation of odor perception in the nose, we performed RNA-sequencing (RNA-seq) in the whole olfactory mucosa (WOM) of the mice fed the CHOW, hpCTR, or hpHFD (Figure 2D). PCA and hierarchical clustering (HC) analyses of the transcriptomic data segregated the samples according to the diets and into two groups: one included all samples from animals fed the grain-based CHOW, and the other comprised the samples from animals fed the two hpCTR and hpHFD (Figure 2E) – congruent with the fact that these two diets similarly impair olfaction (Figures 1 and 2). To gain more insights into the diet-

induced transcriptomic changes, we performed differential expression analysis for all possible dietary pairwise comparisons. The comparisons between CHOW and the hpHFD and hpCTR yielded 4302 and 5789 differentially expressed genes (DEGs), respectively, but the comparison between hpCTR and hpHFD only yielded 103 DEGs (Figure 2F). Next, we focused on the canonical markers of the different cell types populating the WOM. We found subtle enrichment in the expression of markers for mature and immature OSNs (mOSNs and iOSNs, respectively) in WOMs from mice fed an CHOW, and in the expression of horizontal basal cells (HBCs) markers in WOMs from mice fed a hpCTR or hpHFD (Figure S2C).

The changes in the expression of cell markers observed above could reflect differences in the abundance of those specific cell types caused by diet-induced dysregulation of neuroregenerative, inflammatory, or apoptotic processes [25,27,58]. To test this hypothesis, we asked whether genes involved in eliciting neuroregeneration or apoptosis are among the DEGs identified above. First, we looked at genes integrating the NF- κ B-mediated cell survival pathway, which promotes neuroregeneration induced by acute inflammation [59]. We found that 5/13 are differentially expressed between CHOW and hpHFD or hpCTR, with the majority (~80%) being enriched in CHOW compared to hpCTR or hpHFD (Figure 2G). Second, we analyzed the genes composing the intrinsic apoptotic pathway and found that 16/54 are differentially expressed between CHOW and hpHFD or hpCTR, with the majority (~82%) being enriched in hpCTR or hpHFD compared to CHOW (Figure 2H). Together these results suggest that the WOMs of animals fed hpHFD and hpCTR have higher levels of apoptosis than the WOMs of animals fed the CHOW.

To gain deeper and unbiased insights into the functions of all diet-induced DEGs, we performed gene ontology (GO) over-representation analysis (see Methods). We obtained a total of 18, 74, and 12 GO Biological Process categories enriched for the hpHFD vs. CHOW, hpCTR vs. CHOW, and hpHFD vs. hpCTR, respectively (Additional file 3: Table S2). Three of the top five GO-enriched categories for the hpHFD vs. CHOW and hpCTR vs. CHOW comparisons are related to the extracellular matrix and structure organization, with most genes composing these three categories being enriched in CHOW compared to hpCTR or hpHFD (Figure 2I, Additional file 3: Table S2). Interestingly, lower expression levels of extracellular matrix genes are associated with lower numbers of collagen-expressing mesenchymal cells and age-dependent impairment of olfaction [58], suggesting that the WOMs of animals fed an CHOW may have higher regenerative potential than the WOMs of animals fed highly processed diets. In contrast, genes displaying enriched expression in hpCTR or hpHFD compared to CHOW belong to GO categories involved in ATP metabolic processes, oxidative phosphorylation, wound healing, and immune function (Figure 2I, Additional file 3: Table S2); suggesting that the WOMs of animals fed highly processed diets have higher levels of inflammation and tissue damage. Lastly, most categories enriched between HFC and hpCTR are related to the immune system and composed of genes showing enriched expression in hpHFD compared to hpCTR (Figure 2I, Additional file 3: Table S2); thus, suggesting a higher level of inflammatory processes in animals fed hpHFD, which then trigger enhanced immune system responses.

Overall, these results indicate that the short-term consumption of highly processed diets, compared to the more natural CHOW, negatively affects cellular processes regulating neuroregeneration, inflammation, and cell death. This data are consistent with changes observed in aged olfactory epithelia [58–60], and also with previous studies performing long-term dietary interventions [24,25,27].

3.4. Short-term consumption of highly processed diets differentially affect the transcriptional profiles of various brain regions

Internal metabolic signals can also modulate olfaction by acting on the central nervous system (CNS) [12,22,57]. Furthermore, consuming different macronutrients in the diet can modulate gene expression patterns and thereby affect brain physiology [55,61,62]. Our results above indicate that the decrease in responsiveness of OSNs to odors, caused by consuming highly processed diets, only accounts for half of the variation of odor-guided behaviors (Figure 2C). These data suggest the presence of additional modulatory mechanisms in the brain, which are likely regulated by diet-induced changes in gene expression and contribute to the adverse effects of highly processed diets on odor-guided behaviors.

To test this hypothesis, we performed RNA-seq in four broad brain regions — olfactory bulb (OB), brain (BRN, consisting of the cortical and subcortical regions), cerebellum (CBL), and brainstem (BST, which consists of the mesencephalon, pons, and myelencephalon) — of mice fed the CHOW, hpCTR, or hpHFD (Figure 3A, see Methods). As expected, PCA and hierarchical clustering analysis of the transcriptomic data segregated the samples, first according to brain regions and second according to the diet (Figure 3B and S3A).

To gain more insights into the diet-induced transcriptomic changes, we performed differential expression analysis for all possible dietary pairwise comparisons. Across all brain regions, the dietary comparisons yielding the highest number of DEGs were between CHOW and the hpCTR and hpHFD, ranging from 1573 to 7989 DEGs (Figure 3C). The comparison between hpCTR and hpHFD yielded 5466 DEGs for the OB, 8 for BRN, 1 for CBL, and none for BST. Interestingly, of the four brain regions analyzed, the OB registered the highest number of DEGs across all the dietary comparisons (20,687), followed by the BST (8,613), BRN (6,985), and CBL (4,035). Next, we focused on the canonical markers of the major cell types populating the CNS: neurons (NEUs), astrocytes (ASTs), microglia (MCGs), oligodendrocytes (OGDs), oligodendrocyte progenitors (OPCs), and endothelial cells (ENDs) [63–65]. The OB was the brain region with the highest number (37) of cell type markers differentially expressed between the different diets, followed by the BRN and BST, each with 12 DEGs, and the CBL with 9 DEGs (Figure 3D and S3B). Interestingly, most DEGs displaying enriched expression in animals fed the hpHFD or hpCTR were found in the OB, whereas most cell-type markers presenting enriched expression in CHOW are the most abundant in the BST, followed by the BRN and CBL. Among all the cell type markers, the END marker *Ft1* is a notable exception, which consistently shows enriched expression in hpHFD or hpCTR compared to CHOW across brain regions. Interestingly, increased brain expression levels of *Ft1* are associated with neurodegenerative diseases [66,67].

Next, to gain deeper and unbiased insights into the diet-induced DEGs at the functional level, we performed GO over-representation analysis (see Methods). We obtained between 6 and 57, 1–59, and 0–44 GO categories enriched for the hpHFD vs. CHOW, hpCTR vs. CHOW, and hpHFD vs. hpCTR, respectively (Additional file 4: Table S3). For the hpHFD vs. CHOW and hpCTR vs. CHOW comparisons, the GO-enriched categories related to the extracellular matrix and structure organization (OB, BRN, and BST), dynein binding (OB), calcium channel activity (OB), cognition (BRN), or endothelial development (BRN), are composed of genes enriched in animals fed an CHOW. In contrast, GO-enriched categories composed of genes enriched in hpHFD- or hpCTR-fed animals are related to oxidative phosphorylation (OB, BRN, and CBL), ATP metabolism (OB, BRN, and CBL), mitochondrial activity and metabolism (OB, BRN, and CBL), or RNA-splicing mechanisms (CBL,

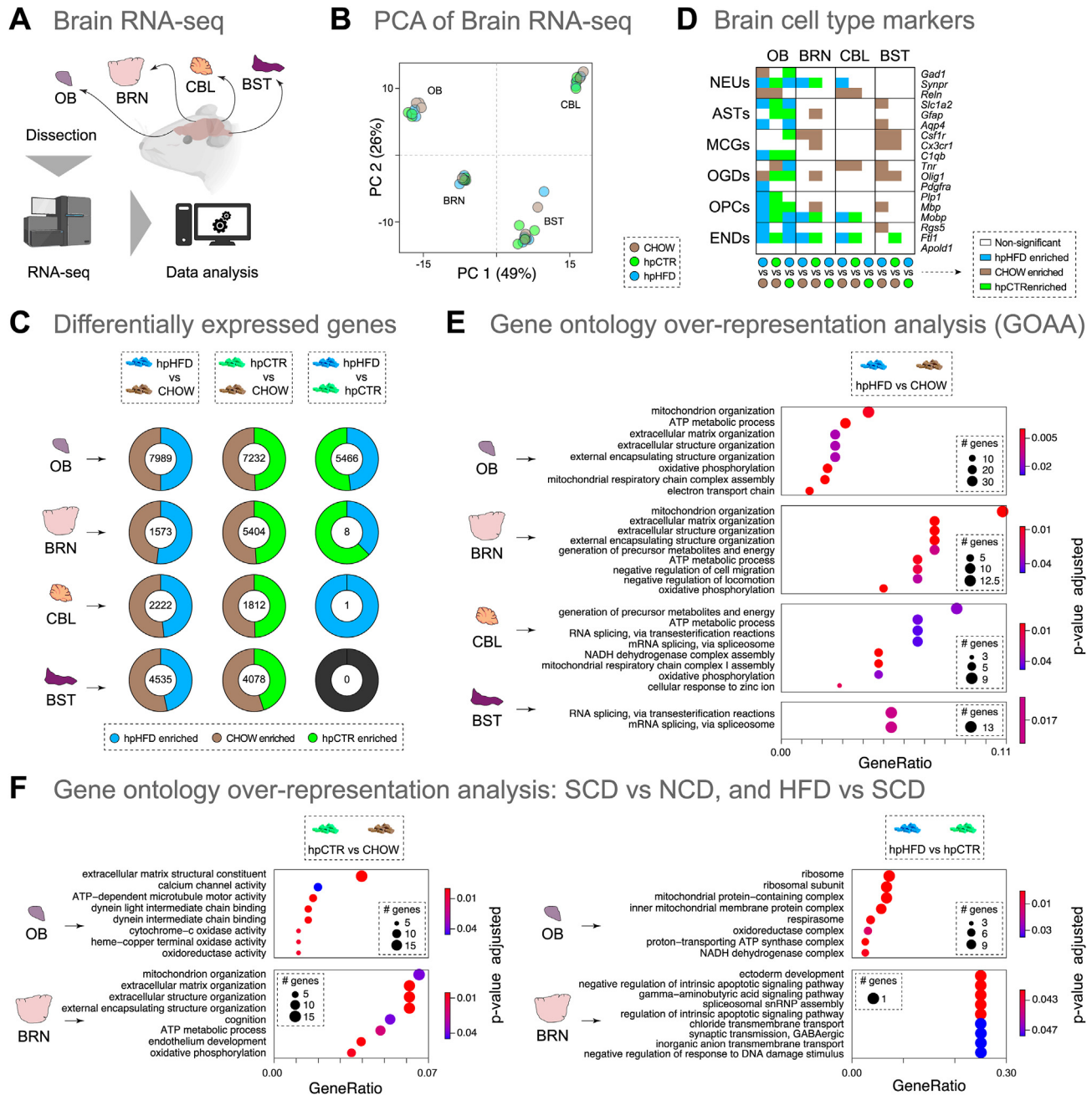


Figure 3: Highly processed diets differentially affect the transcriptome of various brain regions. (A) Schematic view of the RNA-seq experimental strategy for the four broad brain regions: olfactory bulb (OB), brain (BRN, consisting of the cortical and subcortical regions), cerebellum (CBL), and brainstem (BST, which consists of the mesencephalon, pons, and myelencephalon) of mice fed different diets (CHOW, hpCTR or hpHFD; $n = 3-4$ mice per group). (B) Principal-component analysis (PCA) of the union of the top 1000 most expressed genes across all brain regions samples. (C) Pie chart showing the total number and relative proportion of differentially expressed genes (DEGs; $p\text{-adj} < 0.05$) for each pairwise comparison between diets within the different brain regions. Genes enriched in mice fed CHOW, hpCTR or hpHFD are indicated in brown, green or blue, respectively. (D) Heatmap highlighting differentially expressed genes between diets and within different brain regions for known markers of brain cell types (NEUs, neurons; ASTs, astrocytes; MCGs, microglial cells; OGDs, oligodendrocytes; OPCs, oligodendrocyte progenitor cells; ENDS, endothelial cells). DEGs enriched in mice fed CHOW, hpCTR or hpHFD are indicated in brown, green or blue, respectively. Genes with no significant expression changes are represented in white. (E) Dot plot of selected significant Gene Ontology (GO) terms performed on DEGs ($\log_2(\text{FC}) > 1$, $p\text{-adj} < 0.05$) from hpHFD vs. CHOW diet comparison in OB, BRN, CBL or BST regions. (F) Dot plot of selected significant Gene Ontology terms obtained by gene over-representation analysis done on DEGs ($\log_2(\text{FC}) > 1$, $p\text{-adj} < 0.05$) from hpCTR vs. CHOW (left panels) or hpHFD vs. hpCTR (right panels) diet comparisons in OB and BRN regions. Enriched terms are displayed by gene ratio (number of genes related to a GO term/total number of significant genes). The size of the dot reflects the number of genes enriched within the associated GO term, and its color reflects the p-adjusted value for each term.

and BST) (Figure 3E and F, Additional file 4: Table S3). For hpHFD vs. hpCTR comparison, we identified GO-enriched categories composed of genes enriched in animals fed an hpCTR, such as ones related to ribosomal processes in the OB, or RNA-splicing mechanisms in the BRN (Figure 3F, Additional file 4: Table S3). Finally, we also observed GO-enriched categories integrating genes enriched in animals fed an hpHFD, including several related to mitochondrial activity (OB). Together, these data suggest that regardless of their macronutrient composition, short-term ingestion of highly processed diets dysregulate a wide range of gene expression networks across the brain. Interestingly, many of the dysregulated pathways (e.g., extracellular matrix organization, oxidative phosphorylation, mitochondrial activity) are well-known to be associated with neuroinflammation in the brain, increasing the risk of developing neurodegenerative diseases [68].

3.5. Effects of short-term consumption of highly processed diets on weight gain, glucose tolerance, and adiposity

To further investigate the impact of short-term consumption of highly processed diets, we assessed the body weight gain, glucose tolerance, and adiposity levels in mice fed the CHOW, hpCTR, or hpHFD for 30 days in a different animal facility (see Methods, Figure 4A). Mice fed the hpHFD gained significantly more body weight than those fed the CHOW or the hpCTR ($n = 9-10$ per group; two-way repeated measures ANOVA, Time: $F_{(3,75)} = 46.85$, $p < 0.0001$; Diet: $F_{(2,25)} = 17.45$, $p < 0.0001$; Interaction: $F_{(6,75)} = 22.01$, $P < 0.0001$; Figure 4B and S4A). Next, we quantified the weights of the inguinal white adipose tissue (iWAT), gonadal WAT (gWAT), and interscapular brown adipose tissue (iBAT) at the end of the dietary intervention. While mice on the hpHFD showed significantly higher amounts of iWAT and gWAT than those fed the CHOW or the hpCTR, we observed no significant differences for the iBAT ($n = 8-9$ per group; $p < 0.05$, one-way ANOVA, BKY multiple-comparisons correction; Figure S4B). We then investigated the impact of the tested diets on glucose tolerance after 60 and 120 min of intraperitoneal bolus glucose injection. Only mice fed the hpHFD presented glucose intolerance ($n = 6$ per group; two-way ANOVA, Time: $F_{(4,75)} = 42.59$, $p < 0.0001$; Diets: $F_{(2,75)} = 15.57$, $p < 0.0001$; interaction: $F_{(8,75)} = 1.752$, $p = 0.1003$, BKY multiple comparisons correction; Figure 4C), likely due to the interference of diet-derived circulating fats with the insulin receptor, which reduces glucose uptake by peripheral tissues [69,70]. Together, these results show that only the short-term consumption of hpHFD negatively affects body weight, adiposity levels, and glucose tolerance.

3.6. Short-term consumption of highly processed diets affect brain metabolism and connectivity

Despite making only $\sim 2\%$ of the body volume, the brain consumes $\sim 20\%$ of the total glucose-derived energy [71]. This elevated energy consumption rate makes the brain highly sensitive to changes in dietary regimens [72]. *Ex-vivo* studies in rodents have shown that short- and long-term consumption of diets rich in fat or sucrose leads to brain metabolic changes [73–75]. However, whether the short-time consumption of highly processed diets affect brain glucose metabolism remains largely unknown.

To answer these questions, we performed non-invasive brain glucose metabolism assessments with ^{18}F -Fluorodeoxyglucose positron-emission tomography (FDG-PET) brain imaging after 25 days of dietary intervention (Figure 4A and D). Brain FDG-PET is widely used in clinics as an index of synaptic activity [76], and has an unprecedented translational value. We evaluated glucose metabolism in the same four cerebral regions (OB, BRN, CBL, and BST; $n = 9$ per group) for which we performed RNA-seq in the section above. Our analysis revealed regional diet-induced changes in glucose metabolism in the OB and

BST ($p < 0.05$; one-way ANOVA, BKY multiple-comparisons correction; Figure 4E). In these two regions, glial cells are more abundant than neurons [77–79]. Interestingly, the OB of the mice on the hpHFD showed glucose hypermetabolism compared to mice fed the CHOW or the hpCTR, and the BST of mice fed the hpCTR displayed hypermetabolism compared to animals on the CHOW or the hpHFD ($p < 0.05$; one-way ANOVA, BKY multiple-comparisons correction). We highlight that brain imaging was carried out in overnight fasted mice, which implies that the brain metabolic adaptations were long-lasting, and not an effect of glucose levels due to feeding.

Next, to better understand the short-term dietary impact on brain metabolic connectivity, we used the OB, BRN, CBL, and BST as seed points for a network analysis (Figure 4F). The OB and the BRN seed point analyses showed hyperconnectivity in the animals fed the hpCTR and hpHFD, suggesting that these brain regions are consuming glucose in a more synchronized manner. This synchronicity could be due to short-term network adaptations to cope with increased energy substrate availability. Since glial cells outnumber neurons in these regions [77], one could argue that this hypersynchronicity is associated with this brain inflammatory state proposed above. The same analyses were conducted using brain regions enriched in neurons, such as the CBL, as the seed point. While the network exhibited by animals fed the CHOW and hpHFD were similar, the animals fed the hpCTR displayed metabolic network hypersynchronicity. It is intriguing to consider that the metabolic network hypersynchronicity induced by hpHFD may depend on plastic changes occurring in glial cells [46,80–82]. Indeed, changes in brain metabolic connectivity due to astrocyte-specific modulation have been described before [46,80].

Together, these results indicate that the short-term consumption of diets differing in macronutrient origin and composition can modulate regional brain glucose metabolism and metabolic networks, at least on a macro level. To our knowledge, this is the first *in-vivo* evidence of brain glucose hypermetabolism across many brain regions in such short dietary regimens using highly processed diets, likely indicating a state of brain inflammation triggered by glial responses.

3.7. Brain mitochondrial function is mildly affected by short-term dietary interventions

High-resolution respirometry was employed to assess mitochondrial performance in the OB, cortex (CTX), and hypothalamus (HYP) of diet-treated mice, and several parameters associated with mitochondrial and non-mitochondrial respiration were measured (Figure 5A, and S5A). The respiratory acceptor control ratio (RCR, calculated using oxygen consumption in state3/state4) indicates the rate of mitochondria coupling and efficiency and may be altered under injury conditions [83]. We observed no significant differences in the RCR of the different brain regions between mice fed different diets (Figure 5B, and S5A). The uncoupling control ratio (UCR) is an index of the electron transfer system capacity related to the generation of heat by the mitochondria [84,85]. The UCR was not significantly affected in animals on the hpCTR or hpHFD compared with CHOW in the OB or the CTX ($p < 0.05$; one-way ANOVA, BKY multiple-comparisons correction; Figure 5B, and S5B). However, the UCR of the HYP was significantly higher in animals fed the CHOW compared to animals on a hpCTR and hpHFD (one-way ANOVA, BKY multiple-comparisons correction; $F_{(2,15)} = 5.628$, $P = 0.0150$), consistent with the fact that this brain region is a critical regulator of energy metabolism in the brain, and it is highly affected by an overload of fat [8]. For the remaining four parameters linked to mitochondrial oxygen respiration (ATP-linked respiration, proton leak, and maximal respiration), we observed no significant differences in the RCR of the different brain regions between mice fed different diets. In

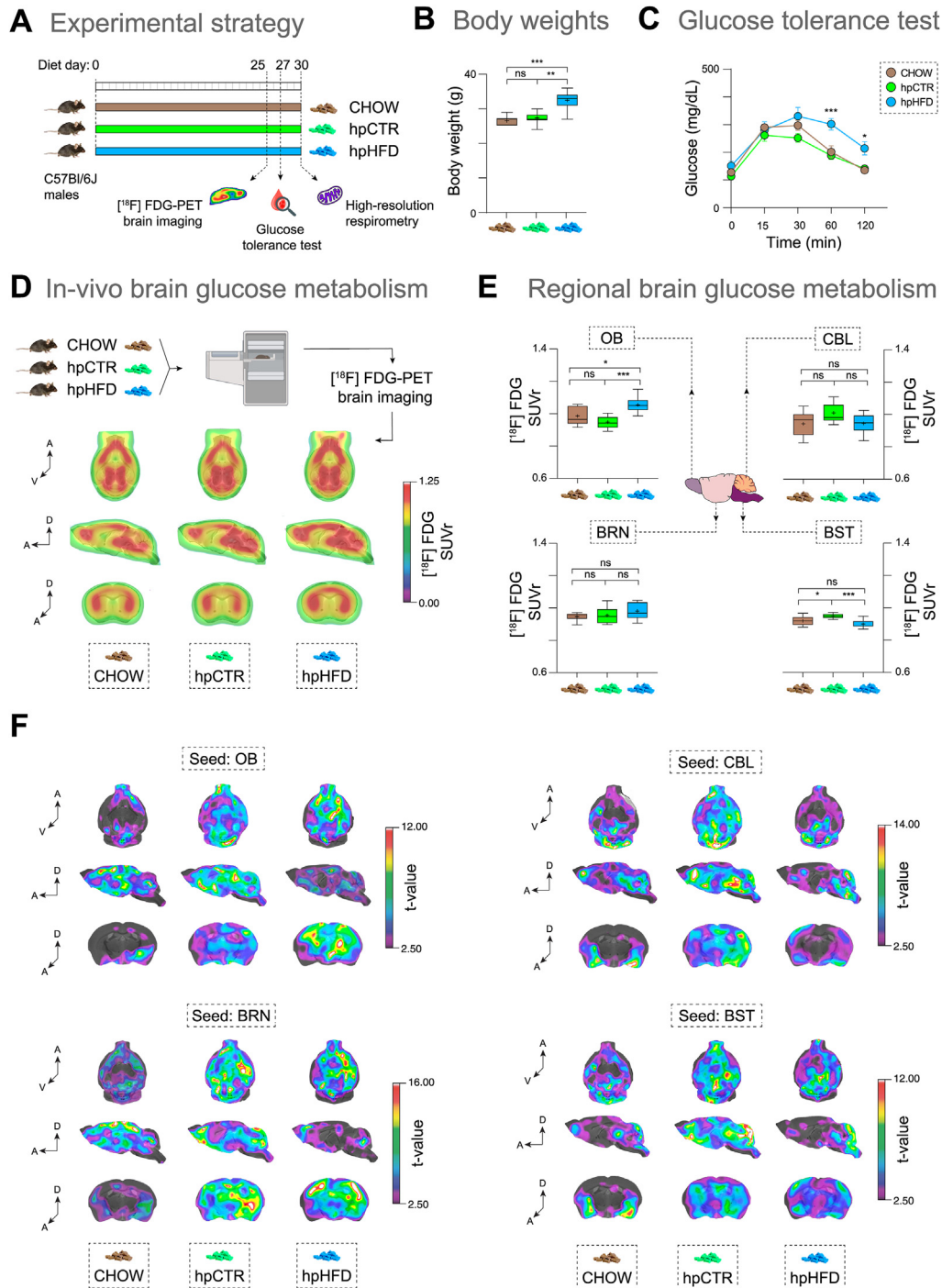


Figure 4: The hpHFD induces metabolic adaptations in the brain. (A) Schematic view of the experimental design for the second part of our study. Mice were fed on different diets (CHOW, hpCTR or hpHFD, $n = 7-8$ mice per group). In vivo brain glucose metabolism was assessed on day 25 of the dietary intervention, with $[^{18}\text{F}]$ -FDG-PET. The glucose tolerance test was performed on day 27. Brain mitochondrial function was analyzed in tissue homogenates on day 30 with high-resolution respirometry. (B) Comparison between the body weight of animals on CHOW, hpCTR or hpHFD ($n = 7-8$ per group). Asterisks indicate significant differences (one-way ANOVA, BKY multiple comparisons correction; ns, non-significant; $**p < 0.01$; $***p < 0.0001$) (C) Glucose tolerance curves for animals on a NCD, SCD, and HFD right before glucose administration ($t = 0$) and 15, 30, 60, and 120 min after an oral glucose administration. Animals fed the hpHFD have higher levels of glucose from minute 30 onwards, when compared with CHOW and hpCTR. Asterisks indicate significant differences (two-way ANOVA, BKY multiple comparisons correction, $n = 6$ per group): ns, non-significant; $*p < 0.05$; $***p < 0.0001$). (D) Metabolic maps showing whole brain $[^{18}\text{F}]$ -FDG metabolism by SUVR of animals on CHOW, hpCTR or hpHFD. The pons region was used as a reference. Warmer colors indicate higher SUVRs. (E) Specific templates for four regions of interest were used to separately quantify regional glucose metabolism in OB, CBL, BRN, and BST. (F) The total brain glucose metabolism was used in a correlation analysis with a specific seed region to estimate glucose metabolism synchronicity between regions. Warmer colors indicate concomitant activation of brain areas and seeding point.

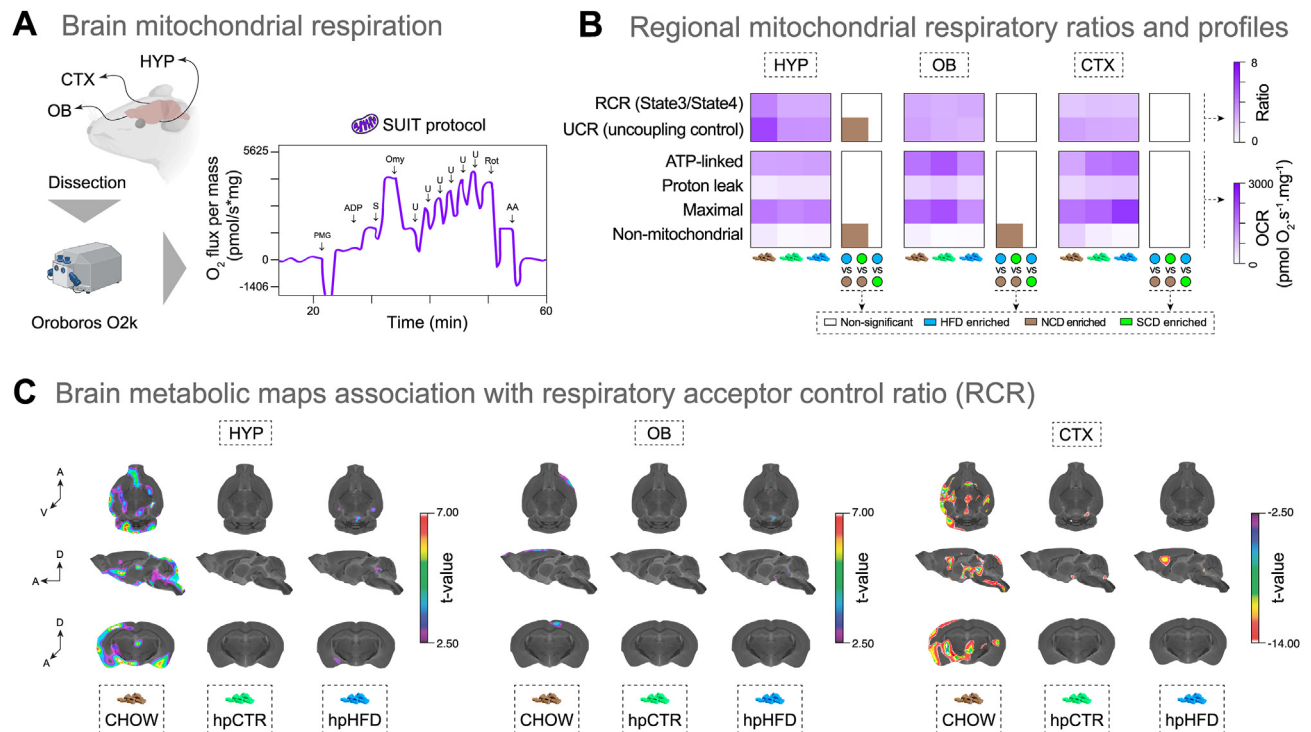


Figure 5: Brain mitochondrial function is mildly affected by the short-term consumption of highly processed diets. (A) Schematic demonstration of brain regions used for high-resolution respirometry. To assess mitochondrial respiration in brain tissue homogenates, a substrate-inhibitor-titration (SUIIT) protocol was used. Oxygen consumption at each stage of the protocol indicates specific mitochondrial properties. Mitochondria control ratios were calculated using the oxygen consumption in state3/state4 (RCR) and maximal respiration/leak (UCR). ATP-linked respiration is considered when all substrates, ADP and oxygen are available for a fully-coupled mitochondrial function. Proton leak measures are made in the presence of an ATP synthase inhibitor. Maximal respiration is achieved by titration with an electron transport system uncoupler. Non-mitochondrial is considered a residual oxygen consumption when the electron transport system and the ATP synthase are inhibited. (B) The HYP, OB, and cortex (CTX) homogenates underwent testing with the SUIIT protocol and had their mitochondrial parameters measured. Heatmap highlighting the mitochondrial functions measured. Similar shades of purple depict similar results. The box to the right of each heatmap indicates the statistical significance of inter-diet comparisons for each parameter ($p < 0.05$; one-way ANOVA, BKY multiple comparisons correction, $n = 4-7$ per group). Comparisons with significantly higher values in CHOW are indicated in brown. Non-significant responses are indicated in white. (C) Using *in vivo* glucose metabolism and the respiratory parameters, we estimated the brain glucose metabolism associations with respiratory acceptor control ratio in each brain region analyzed. Warmer colors indicate a positive correlation between RCR and brain glucose metabolism in the HYP and OB, and a negative correlation between RCR and brain glucose metabolism in the CTX.

the case of the non-mitochondrial oxygen consumption rate (OCR), we only observed significant differences ($p < 0.05$; one-way ANOVA, BKY multiple-comparisons correction) for the HYP and OB, and only when comparing CHOW against hpCTR or hpHFD. Processes related to this non-mitochondrial oxygen expenditure include the activity of oxidase enzymes, oxidation of odd-chain fatty acids, very long fatty acids, and amino acids [86,87]. Under physiological conditions, this is a key process for the reoxidation of NADH, essential to the bioenergetic homeostasis in the cell [88].

Next, we conducted a voxel-wise association analysis integrating glucose metabolism and mitochondrial parameters. Interestingly, the hypothalamic mitochondrial parameters RCR and UCR are associated with hypothalamic (HYP) and cortical (CTX) glucose metabolism in the CHOW group (Figure 5C, and S5C). In contrast, this association is not seen in hpCTR and hpHFD groups. This fact, specifically related to the hypothalamic region, can be a mechanism underlying the loss of homeostatic control the brain has on body weight, commonly seen in individuals consuming a hpHFD. The coupling between glucose metabolism and usage as an oxidative fuel seems abolished due to exposure to hpCTR and hpHFD. No significant associations were found between glucose metabolism and the hypothalamic ROX (Figure S5D), suggesting that the hypothalamic non-mitochondrial usage of oxygen is not coupled to glucose metabolism. We conducted the same analysis with the OB mitochondrial parameters but found no associations

between RCR or UCR and glucose metabolism (Figure 5C, and S5C). In contrast, we found only small significant clusters when analyzing ROX and glucose metabolism, in the OB we found only small significant clusters (Figure S5D). These findings indicate that non-mitochondrial usage of oxygen in this region may have little influence on glucose metabolism in the brain. The cortical RCR was negatively associated with cerebral glucose metabolism in the CHOW group but not in the others. This indicates that the FDG-PET signal is inversely associated with mitochondrial function, suggesting a glucose flux towards the glycolytic pathway independently of mitochondrial coupling. At the cellular level, this energetic flux is classically described in astrocytes, whereas in neurons we expect that lactate would be used for oxidative phosphorylation (and glucose for the pentose phosphate pathway) [89]. Corroborating our previous findings, this association is abolished by short-term hpCTR and hpHFD, which indicates an astrocytic plastic adaptation. Interestingly, the UCR in the CTX is negatively associated with glucose metabolism only in the hpHFD group, which indicates that regions consuming more glucose are likely less prone to deal with mitochondrial stress. This is not seen in the other groups. Regarding OX and glucose metabolism in the CTX, we found only small significant clusters.

Together, these results suggest that the usage of glucose, the main energetic substrate of the brain, is dependent on the nutrients available, and the cell type abundance in a given brain region. The inverse

association between glucose metabolism and mitochondrial function suggests that diet-induced adaptations are mostly driven by astrocytes, which are highly glycolytic cells.

4. DISCUSSION

Previous studies investigating the effects of food on olfaction, brain metabolism, and overall health have predominantly focused on long-term dietary changes involving different macronutrient compositions that result in obesity [12,23–27,72,75]. Here, we provide evidence that short-term consumption of highly processed diets, regardless of macronutrient composition and weight gain, can have profound effects on mouse olfactory physiology and odor-guided behaviors, transcriptional profiles of various cerebral regions, brain metabolism and connectivity, body weight, and glucose tolerance. Our results highlight that even short-term consumption of highly processed foods can trigger early abnormalities in both the peripheral and central nervous systems, thus amplifying the susceptibility to neurological and other non-communicable diseases. Our study further substantiates the idea that the health effects of food are primarily dictated by its matrix, then its nutrient composition, with the quality of calories taking precedence over their quantity [90].

Relative to grain-based chow-fed controls, mice fed the highly processed diets showed substantially altered olfactory preferences and risk assessment episodes, suggesting that the effects of diet on olfactory sensory and cognitive functions may manifest more rapidly than previously thought. These strong diet-induced effects on odor-guided behaviors occurred even in the absence of obesity, in line with a previous study of long-term exposure to a 45 % high-fat diet [26]. Interestingly, obese humans also display altered olfactory preferences and overall lower olfactory sensitivity and function [91,92], but whether the same remains true in non-obese individuals with poor diet or poor metabolic health is unknown. Our results also provide intriguing insights into the potential mechanisms underlying these dietary effects on behavior. The observed impairments in odorant detection (measured by the EOG responses) and the associated behavioral deficits could be attributed to changes in the peripheral detection of odorants in the neuroepithelium of the mouse WOM, possibly mediated by alterations in the response of OSNs to odorants to diet-derived metabolic internal signals [12,22,24,57]. Indeed, our EOG findings are consistent with the impairment of the peripheral detection of odorants in the mouse nose after the long-term consumption of unhealthy high-fat or high-fructose diets [24,27]. Furthermore, the transcriptional responses associated with apoptosis and inflammatory responses in the mouse nose following consumption of highly processed diets suggest that these diets may induce physiological dysregulation of odor perception, possibly through diet-induced dysregulation of neurogenerative, inflammatory, or apoptotic processes [25,27,58–60].

Internal metabolic signals are also powerful regulators of many physiological processes throughout the brain, including key areas involved in the perception of smell and related behaviors, such as the OB, the piriform cortex, and the hypothalamus [12,22,57,93–95]. Our findings align with this, as the electro-olfactogram responses of OSNs to the odorants accounted for about half of the variability in these behaviors, suggesting the involvement of additional modulatory mechanisms in the brain. In this context, the consumption of different macronutrients in the diet is known to modulate gene expression

patterns, thereby affecting brain physiology, and significantly impacting metabolic health and brain function [55,61,62]. In our transcriptomic analyses, we identified DEGs in the WOM and across various brain regions in response to diet consumption, suggesting that the impact of diet on brain function is organ and region-specific. The OB, a key brain region involved in regulating olfactory responses [12,21], registered the highest number of DEGs across all the comparisons (including the WOM), yielding ~53-fold higher number of DEGs for the comparison between the two highly processed diets, thus suggesting that this brain region may be particularly sensitive to dietary interventions and be a key modulator of the olfactory responses. The GO over-representation analysis further revealed that the short-term consumption of highly processed diets dysregulate gene expression networks across the brain, including those related to energy metabolism, oxidative phosphorylation, RNA-splicing, myelination, calcium-channel activity, and others. These findings are consistent with the idea that different diets have distinct effects on different cell types and brain regions, leading to diverse functional outcomes [65,81,96–99].

In rodents, long-term exposure to hpHFD or binge access to a high-sucrose diet can significantly impact brain glucose metabolism and provoke cerebral inflammation, even in the absence of obesity [54,72,74,75,81,98]. In our experiments, the short-term consumption of hpHFD had profound effects on body weight, glucose tolerance, and adiposity levels. In alignment with these findings, our study revealed that short-term consumption of highly processed diets modulates regional brain glucose metabolism and metabolic networks, even in the absence of obesity. This was evidenced by the hypermetabolism observed in the OB and BST of mice fed the hpHFD and hpCTR, respectively. Brain metabolism can react to peripheral cues to adapt its responses depending on external stimuli. Our results indicate that glial cells of OB had their main markers altered by hpHFD and hpCTR, because of diet-induced metabolic alterations. Specifically, the astrocytic marker *Slc1a2* [100], which encodes GLT-1 main trigger for glucose uptake in astrocytes, was altered under the different dietary regimens, which may be directly related to increased glucose metabolism in OB. Moreover, the lack of changes in glucose metabolism in regions where neurons outnumber glial cells (such as the CBL), combined with the fact that glial cells are ultra-plastic in handling glucose [101], suggest that the observed *in-vivo* glucose hypermetabolism in such a short regimen indicates glial adaptive responses. Indeed, recent studies have shown that glial cells contribute to the FDG-PET signal [46,80,82,102]. Thus, such dynamic responses would likely have as their cellular source the glial cells, particularly astrocytes – the most abundant glial cell in the gray matter. These findings suggest that diet can rapidly influence brain function, potentially through mechanisms involving glial cells, which are known to be highly plastic and play a critical role in brain metabolism [103]. Additionally, evidence from clinical studies indicates that early glucose hypermetabolism seen in neurodegenerative disorders is associated with reactive astrogliosis and microglial activation [102,104], suggesting that even short-term consumption of highly processed diets may cause brain inflammatory changes.

Obesity and metabolic syndrome, caused by the long-term consumption of unhealthy diets, can lead to mitochondrial dysfunction in the brain [105,106]. Our findings indicate that short-term dietary interventions can subtly influence brain mitochondrial function, aligning with the early stages of this pathophysiological process. While the

respiratory acceptor control ratio and uncoupling control ratio were not significantly affected in the four broad brain regions, significant changes were observed in the hypothalamus. This suggests that short-term consumption of highly processed diets can influence mitochondrial function in specific brain regions, potentially contributing to the observed changes in brain metabolism and connectivity.

While our study provides novel insights into the impact of short-term highly processed diet consumption on olfactory function and gene expression profiles in various brain regions, there are several limitations to consider. First, our study was conducted in mice, and while they are a widely used model for human diseases, the results may not fully translate to humans (or other species) due to differences in physiology and metabolism. Second, our study was of short duration, and the medium- or long-term effects of these diets on olfactory function and brain gene expression could differ. Third, considering that the mice had unrestricted access to the diets but exhibited varying body weights across diet groups, it would have been beneficial to obtain information on the quantity and energy density of dietary intake. Fourth, we focused on only three diets (CHOW, hpCTR, and hpHFD), leaving the effects of other dietary compositions and content variations unexplored (e.g., macronutrients, micronutrients, fiber, energy density, texture, water content, palatability). We acknowledge that variations in these other factors could potentially account for some or all of the differences between diets we label as “highly processed.” Our aim here was to explore whether any disparities were linked to typically highly processed diets, rather than solely attributing them to food processing. While many of the effects we observed here are associated with the highly processed diets (but not necessarily the processing) discerning the specific components of these three foods responsible for their impact on olfactory behavior and brain function will necessitate further investigation.

5. CONCLUSIONS

In conclusion, our findings highlight the intricate and multifaceted influence of diet on sensory perception, behavior, brain function, and metabolic health. They suggest that diet can swiftly alter brain function, potentially through mechanisms involving the highly adaptable glial cells, which are pivotal in brain metabolism. This underscores the complex interplay between diet and brain function, emphasizing the need for further research to fully understand these relationships. Ultimately, these findings underscore the importance of developing dietary interventions that can enhance metabolic health and optimize brain function, further emphasizing the profound impact of diet on overall health and well-being.

Our findings open several avenues for future research. It would be beneficial to examine the long-term effects of these diets and to investigate the impact of other diet types or variations in macronutrient composition on olfactory function and brain gene expression. Our findings also suggest that, the olfactory system could serve as a potential early indicator or sentinel for the onset of metabolic disorders, is in addition to its recognized role as a biomarker for aging, neurodegenerative issues, and respiratory diseases [107,108]. Additionally, more comprehensive studies are needed to fully understand the cellular and molecular mechanisms underlying the observed changes in olfactory function and brain gene expression. This could involve more in-depth investigations into the role of different cell types and other elements of the brain's gene expression network. Ultimately, a deeper understanding of the impact of diet on olfactory function and brain gene expression could guide the development of dietary interventions to promote health and prevent disease.

ETHICS STATEMENT

The use and care of animals used in this study was approved by the Internal Animal Care and Use Committee (IACUC) of Monell Chemical Senses Center, and by the IACUC of the Universidade Federal do Rio Grande do Sul (UFRGS).

FUNDING

This work was supported by a Sidra Medicine grant (SDR400077, awarded to L.R.S), a Qatar National Research Fund (a member of Qatar Foundation) program grant (JSREP07-016-1-006, awarded to L.R.S), a grant from the Pennsylvania Department of Health (awarded to M.G.T.), the NIH grant 5R01DK124179 (awarded to M.G.T.), the NIH grant 1R01DC016647 (awarded to J.R.), Monell institutional funds, CNPq (312410/2018–2; 435642/2018–9, awarded to E.R.Z), ARD/FAPERGS (21/2551-0000673-0, awarded to E.R.Z), Alzheimer's Association (AARGD-21- 850670, awarded to E.R.Z) and Instituto Serapilheira (Serra-1912-31365, awarded to E.R.Z). Additionally, Monell's animal facility renovations were supported by NIH grant G20-OD020296 for infrastructure improvement. The findings herein reflect the work and are solely the authors' responsibility, and the funders specifically disclaim responsibility for any analyses, interpretations, or conclusions.

AUTHOR'S CONTRIBUTIONS

M.M., D.G.S., S.K., and B.B. performed experiments, analyzed data, and contributed to the writing of the initial version of the manuscript. B.B., H.L., and A.K. performed experiments. A.A.-N., R.H., G.T.V., J.C. da C., S.S.Y.H., N.V., and D.M. analyzed data. J.R., J.M., and M.T. analyzed data, and helped write the manuscript. E.Z. and L.R.S. conceived and supervised the project, analyzed data, and wrote the initial and final versions of the manuscript.

ACKNOWLEDGMENTS

We would like to acknowledge Dr. Amber L. Alhadeff, Dr. Darren W. Logan, Prof. Kunio Kondoh, and the members of the Saraiva Lab and Zimmer Lab for their insightful inputs on data analysis and/or comments on the manuscript. We are thankful to Susie Huang for preliminary bioinformatic analysis, and the Integrated Genomics Services of Sidra Medicine for performing their assistance with the RNA-sequencing.

DECLARATION OF COMPETING INTEREST

The authors declare that they have no known competing financial interests or personal relationships that could have appeared to influence the work reported in this paper.

DATA AVAILABILITY

RNA-seq raw data (Fastq and raw counts files) have been deposited and are publicly available as of the date of publication at GEO under the study accession number GSE218162 (to review GEO accession GSE218162, go to <https://www.ncbi.nlm.nih.gov/geo/query/acc.cgi?acc=GSE218162>, and enter the token 'grangoyojnujodor' into the box). All original code and scripts for the Video Crop tool have been deposited on Github and can be found at <https://github.com/>

NeethuVenugopal/vidocrop. All original code and scripts for the RNA-seq and the brain imaging analyses is available on demand.

APPENDIX A. SUPPLEMENTARY DATA

Supplementary data to this article can be found online at <https://doi.org/10.1016/j.molmet.2023.101837>.

REFERENCES

- [1] Popkin BM. Global nutrition dynamics: the world is shifting rapidly toward a diet linked with noncommunicable diseases. *Am J Clin Nutr* 2006;84(2): 289–98.
- [2] Wiley AS. Chapter 28 - modern human diet. In: Muehlenbein MP, editor. *Basics in human evolution*. Boston: Academic Press; 2015. p. 393–404.
- [3] Albuquerque TG, Bragotto APA, Costa HS. Processed food: nutrition, safety, and public health. *Int J Environ Res Publ Health* 2022;19(24).
- [4] Weaver CM, Dwyer J, Fulgoni 3rd VL, King JC, Leveille GA, MacDonald RS, et al. Processed foods: contributions to nutrition. *Am J Clin Nutr* 2014;99(6): 1525–42.
- [5] McCrickerd K, Forde CG. Sensory influences on food intake control: moving beyond palatability. *Obes Rev* 2016;17(1):18–29.
- [6] Boesveldt S, Parma V. The importance of the olfactory system in human well-being, through nutrition and social behavior. *Cell Tissue Res* 2021;383(1): 559–67.
- [7] Hall KD, Ayuketah A, Brychta R, Cai H, Cassimatis T, Chen KY, et al. Ultra-processed diets cause excess calorie intake and weight gain: an inpatient randomized controlled trial of ad libitum food intake. *Cell Metabol* 2019;30(1): 67–77 e3.
- [8] Loos RJF, Yeo GSH. The genetics of obesity: from discovery to biology. *Nat Rev Genet* 2022;23(2):120–33.
- [9] Kopp W. How western diet and lifestyle drive the pandemic of obesity and civilization diseases. *Diabetes Metab Syndr Obes* 2019;12:2221–36.
- [10] de Araujo TP, de Moraes MM, Magalhaes V, Afonso C, Santos C, Rodrigues SSP. Ultra-processed food availability and noncommunicable diseases: a systematic review. *Int J Environ Res Publ Health* 2021;18(14).
- [11] Gomes Goncalves N, Vidal Ferreira N, Khandpur N, Martinez Steele E, Bertazzi Levy R, Andrade Lotufo P, et al. Association between consumption of ultraprocessed foods and cognitive decline. *JAMA Neurol* 2023;80(2):142–50.
- [12] Palouzier-Paulignan B, Lacroix MC, Aime P, Baly C, Caillol M, Congar P, et al. Olfaction under metabolic influences. *Chem Senses* 2012;37(9):769–97.
- [13] Boesveldt S, de Graaf K. The differential role of smell and taste for eating behavior. *Perception* 2017;46(3–4):307–19.
- [14] Zoon HF, de Graaf C, Boesveldt S. Food odours direct specific appetite. *Foods* 2016;5(1).
- [15] Soria-Gomez E, Bellocchio L, Reguero L, Lepousez G, Martin C, Bendahmane M, et al. The endocannabinoid system controls food intake via olfactory processes. *Nat Neurosci* 2014;17(3):407–15.
- [16] Herz RS. The role of odor-evoked memory in psychological and physiological health. *Brain Sci* 2016;6(3).
- [17] Kontaris I, East BS, Wilson DA. Behavioral and neurobiological convergence of odor, mood and emotion: a review. *Front Behav Neurosci* 2020;14:35.
- [18] Kershaw JC, Mattes RD. Nutrition and taste and smell dysfunction. *World J Otorhinolaryngol Head Neck Surg* 2018;4(1):3–10.
- [19] Kong IG, Kim SY, Kim MS, Park B, Kim JH, Choi HG. Olfactory dysfunction is associated with the intake of macronutrients in Korean adults. *PLoS One* 2016;11(10):e0164495.
- [20] Rawal S, Duffy VB, Berube L, Hayes JE, Kant AK, Li CM, et al. Self-reported olfactory dysfunction and diet quality: findings from the 2011–2014 national health and nutrition examination survey (NHANES). *Nutrients* 2021;13(12).
- [21] Guzman-Ruiz MA, Jimenez A, Cardenas-Rivera A, Guerrero-Vargas NN, Organista-Juarez D, Guevara-Guzman R, et al. Regulation of metabolic health by an “Olfactory-Hypothalamic Axis” and its possible implications for the development of therapeutic approaches for obesity and T2D. *Cell Mol Neurobiol* 2021.
- [22] Jovanovic P, Riera CE. Olfactory system and energy metabolism: a two-way street. *Trends Endocrinol Metabol* 2022;33(4):281–91.
- [23] Lietzau G, Nystrom T, Wang Z, Darsalia V, Patrone C. Western diet accelerates the impairment of odor-related learning and olfactory memory in the mouse. *ACS Chem Neurosci* 2020;11(21):3590–602.
- [24] Riviere S, Soubeyre V, Jarriault D, Molinas A, Leger-Charnay E, Desmoulin L, et al. High Fructose Diet inducing diabetes rapidly impacts olfactory epithelium and behavior in mice. *Sci Rep* 2016;6:34011.
- [25] Chelette BM, Loeven AM, Gatlin DN, Landi Conde DR, Huffstetler CM, Qi M, et al. Consumption of dietary fat causes loss of olfactory sensory neurons and associated circuitry that is not mitigated by voluntary exercise in mice. *J Physiol* 2022;600(6):1473–95.
- [26] Takase K, Tsuneoka Y, Oda S, Kuroda M, Funato H. High-fat diet feeding alters olfactory-, social-, and reward-related behaviors of mice independent of obesity. *Obesity* 2016;24(4):886–94.
- [27] Thiebaud N, Johnson MC, Butler JL, Bell GA, Ferguson KL, Fadool AR, et al. Hyperlipidemic diet causes loss of olfactory sensory neurons, reduces olfactory discrimination, and disrupts odor-reversal learning. *J Neurosci* 2014;34(20):6970–84.
- [28] Monteiro CA, Cannon G, Levy RB, Moubarac JC, Louzada ML, Rauber F, et al. Ultra-processed foods: what they are and how to identify them. *Publ Health Nutr* 2019;22(5):936–41.
- [29] Cootes TA, Bhattacharyya ND, Huang SSS, Daniel L, Bell-Anderson KS, Stifter SA, et al. The quality of energy- and macronutrient-balanced diets regulates host susceptibility to influenza in mice. *Cell Rep* 2022;41(7):111638.
- [30] Kick B. Want to know what to feed mice? *JAX Blog* 2020 02/Oct/2023]. Available from: <https://www.jax.org/news-and-insights/jax-blog/2020/January/mouse-diet-guide>.
- [31] Tremblay AJ, Lamarche B, Guay V, Charest A, Lemelin V, Couture P, et al. Short-term, high-fat diet increases the expression of key intestinal genes involved in lipoprotein metabolism in healthy men. *Am J Clin Nutr* 2013;98(1): 32–41.
- [32] Kuipers EN, Held NM, In Het Panhuis W, Modder M, Ruppert PMM, Kersten S, et al. A single day of high-fat diet feeding induces lipid accumulation and insulin resistance in brown adipose tissue in mice. *Am J Physiol Endocrinol Metab* 2019;317(5):E820–30.
- [33] Wiedemann MS, Wueest S, Item F, Schoenle EJ, Konrad D. Adipose tissue inflammation contributes to short-term high-fat diet-induced hepatic insulin resistance. *Am J Physiol Endocrinol Metab* 2013;305(3):E388–95.
- [34] Edwards LM, Murray AJ, Holloway CJ, Carter EE, Kemp GJ, Codreanu I, et al. Short-term consumption of a high-fat diet impairs whole-body efficiency and cognitive function in sedentary men. *Faseb J* 2011;25(3):1088–96.
- [35] Clara R, Schumacher M, Ramachandran D, Fedele S, Krieger JP, Langhans W, et al. Metabolic adaptation of the small intestine to short- and medium-term high-fat diet exposure. *J Cell Physiol* 2017;232(1):167–75.
- [36] Zeng T, Cui H, Tang D, Garside GB, Wang Y, Wu J, et al. Short-term dietary restriction in old mice rejuvenates the aging-induced structural imbalance of gut microbiota. *Biogerontology* 2019;20(6):837–48.
- [37] Shang Y, Khafipour E, Derakhshani H, Sarna LK, Woo CW, Siow YL, et al. Short term high fat diet induces obesity-enhancing changes in mouse gut microbiota that are partially reversed by cessation of the high fat diet. *Lipids* 2017;52(6):499–511.

- [38] Saraiva LR, Kondoh K, Ye X, Yoon KH, Hernandez M, Buck LB. Combinatorial effects of odorants on mouse behavior. *Proc Natl Acad Sci U S A* 2016;113(23):E3300–6.
- [39] Manoel D, Makhlof M, Arayata CJ, Sathappan A, Da'as S, Abdelrahman D, et al. Deconstructing the mouse olfactory percept through an ethological atlas. *Curr Biol* 2021;31(13):2809–2818 e3.
- [40] Cygnar KD, Stephan AB, Zhao H. Analyzing responses of mouse olfactory sensory neurons using the air-phase electroolfactogram recording. *J Vis Exp* 2010;(37).
- [41] Barrios AW, Nunez G, Sanchez Quinteiro P, Salazar I. Anatomy, histochemistry, and immunohistochemistry of the olfactory subsystems in mice. *Front Neuroanat* 2014;8:63.
- [42] Ruiz Tejada Segura ML, Abou Moussa E, Garabello E, Nakahara TS, Makhlof M, Mathew LS, et al. A 3D transcriptomics atlas of the mouse nose sheds light on the anatomical logic of smell. *Cell Rep* 2022;38(12):110547.
- [43] Kim D, Perteza G, Trapnell C, Pimentel H, Kelley R, Salzberg SL. TopHat2: accurate alignment of transcriptomes in the presence of insertions, deletions and gene fusions. *Genome Biol* 2013;14(4):R36.
- [44] Wang L, Wang S, Li W. RSeQC: quality control of RNA-seq experiments. *Bioinformatics* 2012;28(16):2184–5.
- [45] Love MI, Huber W, Anders S. Moderated estimation of fold change and dispersion for RNA-seq data with DESeq2. *Genome Biol* 2014;15(12):550.
- [46] Rocha A, Bellaver B, Souza DG, Schu G, Fontana IC, Venturin GT, et al. Clozapine induces astrocyte-dependent FDG-PET hypometabolism. *Eur J Nucl Med Mol Imag* 2022;49(7):2251–64.
- [47] Bergeron M, Cadorette J, Tetrault MA, Beaudoin JF, Leroux JD, Fontaine R, et al. Imaging performance of LabPET APD-based digital PET scanners for pre-clinical research. *Phys Med Biol* 2014;59(3):661–78.
- [48] Souza CG, Riboldi BP, Hansen F, Moreira JD, Souza DG, de Assis AM, et al. Chronic sulforaphane oral treatment accentuates blood glucose impairment and may affect GLUT3 expression in the cerebral cortex and hypothalamus of rats fed with a highly palatable diet. *Food Funct* 2013;4(8):1271–6.
- [49] da Silva JS, Nonose Y, Rohden F, Lukaszewicz Ferreira PC, Fontella FU, Rocha A, et al. Guanosine neuroprotection of presynaptic mitochondrial calcium homeostasis in a mouse study with amyloid-beta oligomers. *Mol Neurobiol* 2020;57(11):4790–809.
- [50] Pesta D, Gnaiger E. High-resolution respirometry: OXPHOS protocols for human cells and permeabilized fibers from small biopsies of human muscle. *Methods Mol Biol* 2012;810:25–58.
- [51] Brand MD, Nicholls DG. Assessing mitochondrial dysfunction in cells. *Biochem J* 2011;435(2):297–312.
- [52] Eudave DM, BeLow MN, Flandreau EI. Effects of high fat or high sucrose diet on behavioral-response to social defeat stress in mice. *Neurobiol Stress* 2018;9:1–8.
- [53] Arnold SE, Lucki I, Brookshire BR, Carlson GC, Browne CA, Kazi H, et al. High fat diet produces brain insulin resistance, synaptodendritic abnormalities and altered behavior in mice. *Neurobiol Dis* 2014;67:79–87.
- [54] Kothari V, Luo Y, Tornabene T, O'Neill AM, Greene MW, Geetha T, et al. High fat diet induces brain insulin resistance and cognitive impairment in mice. *Biochim Biophys Acta, Mol Basis Dis* 2017;1863(2):499–508.
- [55] Sarangi M, Dus M. Creme de la Creature: dietary influences on behavior in animal models. *Front Behav Neurosci* 2021;15:746299.
- [56] Parma V, Ohla K, Veldhuizen MG, Niv MY, Kelly CE, Bakke AJ, et al. More than smell-COVID-19 is associated with severe impairment of smell, taste, and chemesthesis. *Chem Senses* 2020;45(7):609–22.
- [57] Bryce B, Baly C, Meunier N. Modulation of olfactory signal detection in the olfactory epithelium: focus on the internal and external environment, and the emerging role of the immune system. *Cell Tissue Res* 2021;384(3):589–605.
- [58] Ueha R, Shichino S, Ueha S, Kondo K, Kikuta S, Nishijima H, et al. Reduction of proliferating olfactory cells and low expression of extracellular matrix genes are hallmarks of the aged olfactory mucosa. *Front Aging Neurosci* 2018;10:86.
- [59] Chen M, Reed RR, Lane AP. Acute inflammation regulates neuroregeneration through the NF-kappaB pathway in olfactory epithelium. *Proc Natl Acad Sci U S A* 2017;114(30):8089–94.
- [60] Robinson AM, Conley DB, Shinnors MJ, Kern RC, et al. Apoptosis in the aging olfactory epithelium. *Laryngoscope* 2002;112(8 Pt 1):1431–5.
- [61] Vaziri A, Dus M. Brain on food: the neuroepigenetics of nutrition. *Neurochem Int* 2021;149:105099.
- [62] Ravi S, Schilder RJ, Kimball SR. Role of precursor mRNA splicing in nutrient-induced alterations in gene expression and metabolism. *J Nutr* 2015;145(5):841–6.
- [63] De Jager PL, Srivastava G, Lunnon K, Burgess J, Schalkwyk LC, Yu L, et al. Alzheimer's disease: early alterations in brain DNA methylation at ANK1, BIN1, RHBDL2 and other loci. *Nat Neurosci* 2014;17(9):1156–63.
- [64] McKenzie AT, Wang M, Hauberg ME, Fullard JF, Kozlenkov A, Keenan A, et al. Brain cell type specific gene expression and Co-expression network architectures. *Sci Rep* 2018;8(1):8868.
- [65] Bondareva O, Rodriguez-Aguilera JR, Oliveira F, Liao L, Rose A, Gupta A, et al. Single-cell profiling of vascular endothelial cells reveals progressive organ-specific vulnerabilities during obesity. *Nat Metab* 2022;4(11):1591–610.
- [66] David S, Jhelum P, Ryan F, Jeong SY, Kroner A, et al. Dysregulation of iron homeostasis in the central nervous system and the role of ferroptosis in neurodegenerative disorders. *Antioxidants Redox Signal* 2022;37(1–3):150–70.
- [67] Kim YK, Jung YS, Song J. Transcriptome profile in the mouse brain of hepatic encephalopathy and alzheimer's disease. *Int J Mol Sci* 2022;24(1).
- [68] Picca A, Calvani R, Coelho-Junior HJ, Landi F, Bernabei R, Marzetti E, et al. Mitochondrial dysfunction, oxidative stress, and neuroinflammation: intertwined roads to neurodegeneration. *Antioxidants* 2020;9(8).
- [69] Shulman GI. Cellular mechanisms of insulin resistance. *J Clin Invest* 2000;106(2):171–6.
- [70] Sears B, Perry M. The role of fatty acids in insulin resistance. *Lipids Health Dis* 2015;14:121.
- [71] Magistretti PJ, Allaman I. A cellular perspective on brain energy metabolism and functional imaging. *Neuron* 2015;86(4):883–901.
- [72] Iozzo P, Guzzardi MA. Imaging of brain glucose uptake by PET in obesity and cognitive dysfunction: life-course perspective. *Endocr Connect* 2019;8(11):R169–83.
- [73] Jais A, Solas M, Backes H, Chaurasia B, Kleinriders A, Theurich S, et al. Myeloid-cell-derived VEGF maintains brain glucose uptake and limits cognitive impairment in obesity. *Cell* 2016;166(5):1338–40.
- [74] Estadella D, Oyama LM, Bueno AA, Habitante CA, Souza GI, Ribeiro EB, et al. A palatable hyperlipidic diet causes obesity and affects brain glucose metabolism in rats. *Lipids Health Dis* 2011;10:168.
- [75] Patkar OL, Mohamed AZ, Narayanan A, Mardon G, Cowin G, Bhalla R, et al. A binge high sucrose diet provokes systemic and cerebral inflammation in rats without inducing obesity. *Sci Rep* 2021;11(1):11252.
- [76] Stoessl AJ. Glucose utilization: still in the synapse. *Nat Neurosci* 2017;20(3):382–4.
- [77] Herculano-Houzel S. The glia/neuron ratio: how it varies uniformly across brain structures and species and what that means for brain physiology and evolution. *Glia* 2014;62(9):1377–91.
- [78] Bandeira F, Lent R, Herculano-Houzel S. Changing numbers of neuronal and non-neuronal cells underlie postnatal brain growth in the rat. *Proc Natl Acad Sci U S A* 2009;106(33):14108–13.
- [79] von Bartheld CS, Bahney J, Herculano-Houzel S. The search for true numbers of neurons and glial cells in the human brain: a review of 150 years of cell counting. *J Comp Neurol* 2016;524(18):3865–95.

- [80] Zimmer ER, Parent MJ, Souza DG, Leuzu A, Lecrux C, Kim HI, et al. [(18)F] FDG PET signal is driven by astroglial glutamate transport. *Nat Neurosci* 2017;20(3):393–5.
- [81] Garcia-Caceres C, Quarta C, Varela L, Gao Y, Gruber T, Legutko B, et al. Astrocytic insulin signaling couples brain glucose uptake with nutrient availability. *Cell* 2016;166(4):867–80.
- [82] Zimmer ER, Pascoal TA, Rosa-Neto P, Nordberg A, Pellerin L. Comment on “Microglial activation states drive glucose uptake and FDG-PET alterations in neurodegenerative diseases. *Sci Transl Med* 2022;14(659):eabm8302.
- [83] Gilmer LK, Ansari MA, Roberts KN, Scheff SW. Age-related mitochondrial changes after traumatic brain injury. *J Neurotrauma* 2010;27(5):939–50.
- [84] Demine S, Renard P, Arnould T. Mitochondrial uncoupling: a key controller of biological processes in physiology and diseases. *Cells* 2019;8(8).
- [85] Gnaiger E. Mitochondrial pathways and respiratory control. An Introduction to OXPHOS Analysis. 5th ed. *Bioenerg Commun*; 2020. p. 2020.
- [86] Chacko BK, Kramer PA, Ravi S, Benavides GA, Mitchell T, Dranka BP, et al. The Bioenergetic Health Index: a new concept in mitochondrial translational research. *Clin Sci (Lond)* 2014;127(6):367–73.
- [87] Banh RS, Iorio C, Marcotte R, Xu Y, Cojocari D, Rahman AA, et al. PTP1B controls non-mitochondrial oxygen consumption by regulating RNF213 to promote tumour survival during hypoxia. *Nat Cell Biol* 2016;18(7):803–13.
- [88] Herst PM, Tan AS, Scarlett DJ, Berridge MV, et al. Cell surface oxygen consumption by mitochondrial gene knockout cells. *Biochim Biophys Acta* 2004;1656(2–3):79–87.
- [89] Pellerin L, Magistretti PJ. Sweet sixteen for ANLS. *J Cerebr Blood Flow Metabol* 2012;32(7):1152–66.
- [90] Fardet A, Rock E. Chronic diseases are first associated with the degradation and artificialization of food matrices rather than with food composition: calorie quality matters more than calorie quantity. *Eur J Nutr* 2022;61(5):2239–53.
- [91] Stafford LD, Whittle A. Obese individuals have higher preference and sensitivity to odor of chocolate. *Chem Senses* 2015;40(4):279–84.
- [92] Velluzzi F, Deledda A, Onida M, Loviselli A, Crnjar R, Sollai G. Relationship between olfactory function and BMI in normal weight healthy subjects and patients with overweight or obesity. *Nutrients* 2022;14(6).
- [93] Al Koborssy D, Palouzier-Paulignan B, Canova V, Thevenet M, Fadool DA, Julliard AK. Modulation of olfactory-driven behavior by metabolic signals: role of the piriform cortex. *Brain Struct Funct* 2019;224(1):315–36.
- [94] Nogi Y, Ahasan MM, Murata Y, Taniguchi M, Sha MFR, Ijichi C, et al. Expression of feeding-related neuromodulatory signalling molecules in the mouse central olfactory system. *Sci Rep* 2020;10(1):890.
- [95] Horio N, Liberles SD. Hunger enhances food-odour attraction through a neuropeptide Y spotlight. *Nature* 2021;592(7853):262–6.
- [96] Duking T, Spieth L, Berghoff SA, Piepkorn L, Schmidke AM, Mitkovski M, et al. Ketogenic diet uncovers differential metabolic plasticity of brain cells. *Sci Adv* 2022;8(37):eabo7639.
- [97] Garcia-Caceres C, Balland E, Prevot V, Luquet S, Woods SC, Koch M, et al. Role of astrocytes, microglia, and tanycytes in brain control of systemic metabolism. *Nat Neurosci* 2019;22(1):7–14.
- [98] Jais A, Solas M, Backes H, Chaurasia B, Kleinridders A, Theurich S, et al. Myeloid-cell-derived VEGF maintains brain glucose uptake and limits cognitive impairment in obesity. *Cell* 2016;165(4):882–95.
- [99] Munji RN, Soung AL, Weiner GA, Sohet F, Semple BD, Trivedi A, et al. Profiling the mouse brain endothelial transcriptome in health and disease models reveals a core blood-brain barrier dysfunction module. *Nat Neurosci* 2019;22(11):1892–902.
- [100] Perego C, Vanoni C, Bossi M, Massari S, Basudev H, Longhi R, et al. The GLT-1 and GLAST glutamate transporters are expressed on morphologically distinct astrocytes and regulated by neuronal activity in primary hippocampal cocultures. *J Neurochem* 2000;75(3):1076–84.
- [101] Magistretti PJ. Neuron-glia metabolic coupling and plasticity. *J Exp Biol* 2006;209(Pt 12):2304–11.
- [102] Xiang X, Wind K, Wiedemann T, Blume T, Shi Y, Briel N, et al. Microglial activation states drive glucose uptake and FDG-PET alterations in neurodegenerative diseases. *Sci Transl Med* 2021;13(615):eabe5640.
- [103] Jha MK, Morrison BM. Glia-neuron energy metabolism in health and diseases: new insights into the role of nervous system metabolic transporters. *Exp Neurol* 2018;309:23–31.
- [104] Salvado G, Mila-Aloma M, Shekari M, Ashton NJ, Operto G, Falcon C, et al. Reactive astrogliosis is associated with higher cerebral glucose consumption in the early Alzheimer’s continuum. *Eur J Nucl Med Mol Imag* 2022;49(13):4567–79.
- [105] Cavaliere G, Trinchese G, Penna E, Cimmino F, Pirozzi C, Lama A, et al. High-fat diet induces neuroinflammation and mitochondrial impairment in mice cerebral cortex and synaptic fraction. *Front Cell Neurosci* 2019;13:509.
- [106] Schmitt LO, Gaspar JM. Obesity-induced brain neuroinflammatory and mitochondrial changes. *Metabolites* 2023;13(1).
- [107] Dan X, Wechter N, Gray S, Mohanty JG, Croteau DL, Bohr VA. Olfactory dysfunction in aging and neurodegenerative diseases. *Ageing Res Rev* 2021;70:101416.
- [108] Gerkin RC, Ohla K, Veldhuizen MG, Joseph PV, Kelly CE, Bakke AJ, et al. Recent smell loss is the best predictor of COVID-19 among individuals with recent respiratory symptoms. *Chem Senses* 2021:46.